ELSEVIER

Precambrian Research 93 (1999) 153–180

Precambrian Research

^{40}Ar–^{39}Ar and Rb–Sr geochronology of the Uruguayan dike swarm, Rio de la Plata Craton and implications for Proterozoic intraplate activity in western Gondwana

Wilson Teixeira [a,*], Paul R. Renne [b], Jorge Bossi [c], Nestor Campal [c], Manoel S. D'Agrella Filho [d]

[a] *Geochronological Research Center-CPGeo, Instituto de Geociências, Universidade de São Paulo, P.O. Box 11348, 05422-970 São Paulo, SP, Brazil*

[b] *Berkeley Geochronology Center, 2455 Ridge Road, Berkeley, CA 94709, USA*

[c] *Faculdad de Agronomia, Universidad de la Republica, Montevideo, Uruguay*

[d] *Instituto Astronômico e Geofísico, Universidade de São Paulo, P.O. Box 9638, 04301-002 São Paulo, SP, Brazil*

Received 9 December 1997; accepted 22 July 1998

Abstract

The Uruguayan dike swarm intrudes country rocks of the Rio de la Plata Craton that were deformed and metamorphosed to high grade during the 2200–1900 Ma Transamazonian orogeny. Slow cooling of the continental crust following this event is suggested by the ^{40}Ar–^{39}Ar plateau ages of hornblende (2016 ± 11 Ma) and biotite (1817 ± 10 Ma) from the Pintos post-tectonic granodiorite.

There are seven ^{40}Ar–^{39}Ar age determinations on mafic dikes and felsic veins from the swarm between 1727 and 1700 Ma. One dike yielded concordant plateau ages for igneous hornblende (1727 ± 10 Ma) and biotite (1725 ± 10 Ma). These ages are taken as the best estimate for the emplacement of the Uruguayan swarm. A Rb–Sr whole rock best fit line calculated for 15 dikes yielded 1766 ± 124 Ma, in agreement (within error) with the ^{40}Ar–^{39}Ar plateau ages.

The origin of the Uruguayan swarm is tectonically related to the emplacement of the Illescas and Minas de Corrales rapakivi granites that crop out in the Nico Perez domain. The tectonic setting of these units is also compatible with bimodal magmatism and basin formation associated with extensional events in the Uruguayan and Brazilian shields. On the whole, the geologic framework suggests that the Uruguayan dike swarm marks a transcontinental intraplate episode within the South America continent which occurred shortly after the Transamazonian orogeny.

The results of initial release portions of ^{40}Ar–^{39}Ar spectra (dikes and felsic veins) coupled with a Rb–Sr mineral isochron from one felsic vein are between 1370 and 1170 Ma. Eight K–Ar ages range from 1600 to 1170 Ma, suggesting variable argon loss in the systems. These isotopic disturbances were probably favored by low-grade hydrothermal overprints, exemplified by differences in the ^{40}Ar–^{39}Ar spectra from one felsic vein (muscovite and biotite), and suggested also by the secondary mineralogy that may be present in the dikes. These post-emplacement ages could result from Mesoproterozoic crustal shortening, recognized in the Nico Perez domain, interpreted to be tectonically associated with the Namaqua orogeny of Southern Africa. This inference is important in understanding the Late Mesoproterozoic evolution of Western Gondwana and brings potential implications for a paleogeographic reconstruction between the paleocontinent Plata and Amazonia at the time of the Grenville orogeny.

Keywords: Dikes; Proterozoic; Gondwana

* Corresponding author. Tel: +55 11 818 3906; Fax: +55 11 818 3993; e-mail: wteixeir@usp.br

0301-9268/99/$ – see front matter
PII S0301-9268(98)00087-4

1. Introduction

Geochronological knowledge in many cratons supports the idea that Paleoproterozoic protocontinents coalesced into large, relatively stable continental masses whose behavior was compatible with a more rigid lithosphere (e.g. Windley, 1984). It is also believed (e.g. Gurnis, 1988) that aggregation and dispersal of continental plates are controlled by a dynamic feedback between the plate and mantle convection, and that fragmentation of the rigid lithosphere is induced by the episodic hot upwelling of newly created isotherms within the asthenosphere. Proterozoic mafic dike swarms that are common in many cratons can provide relevant information on geodynamic processes responsible for their genesis and emplacement. Consequently they have an important bearing on the geologic evolution of continents, constraining the time of extensional episodes that can be genetically associated with igneous activity.

In South America, the Transamazonian orogeny (2200–1900 Ma) played an important role in the coalescence of Archean fragments, and eventually led to the formation of large continental masses (e.g. Cordani et al., 1988). These were later intruded by several generations of dike swarms, and most of them have been investigated by means of paleomagnetism, petrology, geochemistry and geochronology (e.g. D'Agrella Filho et al., 1990; Renne et al., 1990; Bellieni et al., 1991, 1995).

One of the most extensive swarms, the Uruguayan dike swarm (UDS; Fig. 1), occurs in the Rio de la Plata Craton (RLPC). Recent investigations have presented the geological, petrographic, geochemical and petrologic characteristics of this swarm, composed of tholeiitic andesites and andesitic basalts (Bossi and Campal, 1991; Rivalenti et al., 1991; Bossi et al., 1993; Mazzucchelli et al., 1995).

Bossi et al. (1993) first reported a Rb–Sr whole rock isochron age of 1861 ± 125 Ma and $^{87}Sr/^{86}Sr$ initial ratio (Sr_0) of 0.7031 (MSWD = 1.29) for 14 dikes of the swarm, interpreted to be the approximate time of emplacement. This result agrees within error with two K–Ar biotite ages (1828 ± 21 Ma and 1786 ± 26 Ma; Table 1) on country rocks in sharp contact with the dikes. Nevertheless, K–Ar dates on plagioclase and whole rock from eight dikes are between 1600 and 1170 Ma (see Table 1), suggesting variable argon loss from the systems.

This paper presents the first ^{40}Ar–^{39}Ar data on minerals and Rb–Sr determinations on whole rocks and mineral concentrates for the UDS. These results broadly support the Rb–Sr whole rock geochronological study of Bossi et al. (1993), refine the dikes' emplacement age and provide insights on their subsequent thermal history. The tectonic significance of the Uruguayan swarm is presented in the context of fragmentation of the South American continental mass (including both basin sedimentation and magmatism) post-dating the Transamazonian orogeny.

2. Geologic setting

Three main geotectonic units make up the Uruguayan Precambrian shield (Fig. 1): the Paleoproterozoic granite–gneissic terrain of the RLPC in the west; the Nico Perez polyphase domain; and the Neoproterozoic eastern domain. These domains extend to the north and south of Uruguay, in southern Brazil and parts of Argentina, respectively (e.g. Cordani et al., 1974). The main episode of metamorphism and deformation in eastern Uruguay is related to the Brazilian orogeny during which granite–gneiss–migmatite terrains intruded by syn-, late- and post-tectonic granites were formed between 680 and 500 Ma (Ferrando and Fernandez, 1971; Umpierre and Halpern, 1971; Bossi, 1983; Soliani, 1986; Fragoso Cesar, 1991). These rocks constitute the major NE–SW trending Dom Feliciano belt which connects to the Gariep and Damara belts in southern Africa — a result from West Gondwana assembly during Neoproterozoic to Early Paleozoic times.

The RLPC comprises extensive granite–gneiss terrains, migmatites and metasedimentary belts that were strongly deformed during the Transamazonian orogeny (Bossi et al., 1996; Campal, 1990). Rocks of different compositions intrude the country rocks and the metasedimentary belts, and some of them are stratified basic bodies and stocks (e.g. Fernandez and Preciozzi, 1974;

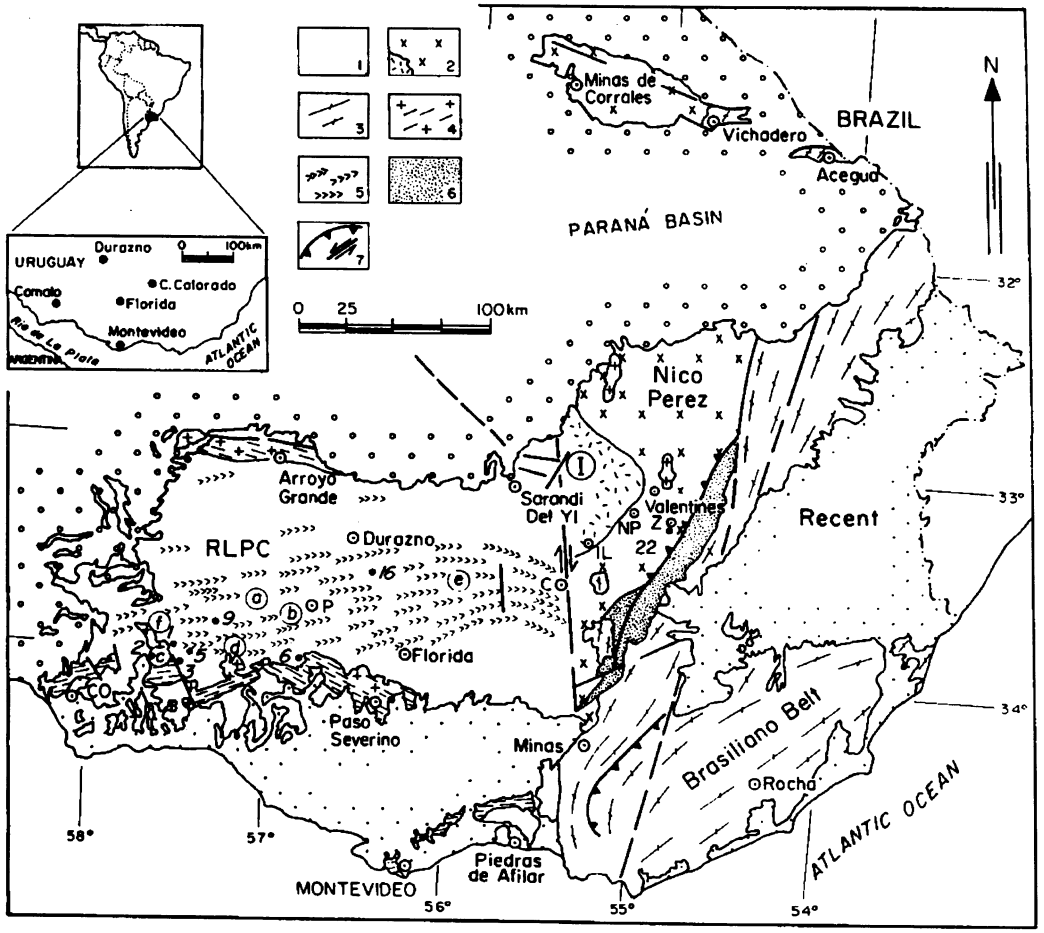

Fig. 1. Geologic outline of the investigated area [adapted from Dalla Salda et al. (1988) and Bossi et al. (1993); Campal and Schipilov (1995)]. 1, RLPC, Rio de la Plata Craton (Paleoproterozoic). 2, The Proterozoic Nico Perez polycyclic domain and the Illescas rapakivi granite (I). 3, Brazilian domain of Eastern Uruguay. Geological units: 4, metasedimentary belts and intrusive granites of Paleoproterozoic age; 5, UDS. Mylonitic belts (6) and major faults and lineaments (7) of the Nico Perez domain are also shown. The NW–SE dashed line in the Paraná basin represents the geophysical anomaly inferred by Hallinan et al. (1993). Numbers in the RLPC indicate the sites of samples dated in this study (e.g. 1, U-201; 2, U-202; 16, U-216; 22, U-222). Italic letters (*a–e*) locate the K–Ar dates of the UDS (Table 1); $f=1930$ Ma granitoid (Ferrando and Fernandez, 1971). See text for details. Key words: P, Pintos granodiorite; NP, Nico Perez; Il, Illescas; Z, Zapican; C, Cerro Colorado; and CO, Carmelo cities.

Bossi and Navarro, 1988; Dalla Salda et al., 1988). Reconnaissance Rb–Sr and K–Ar geochronology on whole rocks and muscovites from the gneisses and granitic intrusives (Hart, 1966; Ferrando and Fernandez, 1971; Umpierre and Halpern, 1971) yielded ages in the range of 2100–1830 Ma [re-calculated with the decay constants recommended by Steiger and Jäger (1977)]. More recent Rb–Sr work on several syn-tectonic and post-tectonic granitoids intrusive into the supracrustal belts have yielded ages between 2290 and 1990 Ma. Most of these isochrons cluster at 1988 ± 16 Ma, indicating the link of the plutons with the Transamazonian orogeny (Cingolani et al., 1990, 1997; Precciozi and Bourne, 1992).

The main Transamazonian deformation of the country rocks also affected the supracrustal belts (Campal, 1990). During early deformation, ENE

Table 1
K–Ar age determinations on the mafic dikes (UDS) and country rocks of the western part of Uruguayan shield

Unit	Sample/material	%K	$^{40}Ar_{rad}$	% $^{40}Ar_{atm}$	Age (Ma)	Observations[a]
Country rock	U-19/biot	6.82	837.8	1.6	1828±21	1
Country rock	U-26/biot	6.89	818.6	0.4	1786±26	1
Nico Perez	U-91.1/musc	8.75	614.6	6.2	1253±32	2
UDS	DR19/plag	2.60	259.1	2.7	1595±36	3a[b]
UDS	DR333/WR	1.65	140.5	2.3	1435±25	3b
UDS	U-89.1/WR	0.81	69.8	7.4	1495±41	4
UDS	U-89.3/WR	0.16	13.6	35.8	1514±85	4
UDS	U-89.9/WR	1.59	97.8	3.0	1171±35	4
UDS	01(002)/WR	1.38	138.9	0.9	1604±40	5c
UDS	02(012)/WR	1.55	124.1	1.9	1373±33	5d
UDS	03(015)/WR	1.27	103.4	1.1	1393±44	5e

rad, Radiogenic argon (10^{-6} ccSTP g^{-1}); atm, atmospheric argon; plag, plagioclase; WR, whole rock; biot, biotite; musc, muscovite.
[a]Observations: 1, country rock in sharp contact with the dikes; (Bossi et al., 1993); 2, mylonite; Nico Perez domain (Campal et al., 1995); 3, unpublished data (CPGeo/USP cooperative project with E. Medina); 4, unpublished data (CPGeo/USP cooperative project with R.Varela, C. Cingolani and J. Bossi); and 5, Gomez Rifas (1988).
[b]Sample locations available (a, b, c, d, e) are shown in Fig. 1.

trending structures associated with isoclinal folding were formed. Furthermore, two younger tectonothermal episodes have overprinted the country rocks. The older episode produced major E–W structures represented by folding of mylonitic surfaces, whilst the second, ductile, episode generated NW structures, in association with abundant intrusions of microgranites, quartz–feldspar veins and pegmatites. During the second episode intense thermal activity also caused anatexis of the RLPC country rocks.

The Nico Perez domain is composed of granitoid complexes and granulitic gneisses (e.g. Valentines). To the north, in the Minas de Corrales–Vichadero region (Fig. 1), high grade gneisses are also exposed. They yield a Rb–Sr isochron age of 2204±65 Ma, indicating the tectonic association with the Transamazonian orogeny. Around Minas de Corrales (Fig. 1), rapakivi granites have been recently mapped overlain by supracrustal rocks of Mesoproterozoic age (F. Precciozi; personal communication, 1998), and a Rb–Sr age calculation using samples located in the area where the rapakivi granites and associated rocks crop out yields an isochron of 1777±60 Ma [data recalculated from Cordani and Soliani (1990)].

The Nico Perez domain exhibits a more complex geologic evolution compared to the granite–gneissic terrain that crops out to the west of the NNW–SSE Sarandi Del Yi fault (see Fig. 1). The tectonic framework of the domain is illustrated by the presence of extensive mylonitic zones, as well as co-existence of supracrustal relics and medium- to high grade rocks, partly reworked during Meso- and Neoproterozoic events. These features indicate that the Nico Perez domain represents the Paleoproterozoic cratonic edge partially reworked by younger Precambrian events (e.g. Dalla Salda et al., 1988; Campal et al., 1995; Gaucher et al., 1996).

A similar tectonic situation is observed in the Tijucas belt (not shown) — the physical prolongation of the Nico Perez domain in southern Brazil. This belt is characterized by granite–gneissic relics of the Paleoproterozoic age (Cordani et al., 1974) and a rift-related Mesoproterozoic metavolcanic-sedimentary sequence (Porongos Group) intruded by granites, alkaline rocks and anorthosites of different ages, further deformed and metamorphosed during the Brazilian orogeny (e.g. Babinski et al., 1996, 1997). It is noteworthy that the Neoproterozoic granites which intrude into the Tijucas belt (as well as into the Dom Feliciano belt located to the east) have T_{DM} model ages (2.0; 1.31–1.41 and 1.58–1.75 Ga) indicating that they may represent either the direct melting

of a Paleoproterozoic crust or mixtures of Mesoproterozoic and Brazilian materials (Babinski et al., 1997).

Along the eastern sector of the Nico Perez domain in Uruguay SE folds and related low dip thrusts indicate the transport of the country rocks to the southeast. A K–Ar age of 1253 ± 32 Ma (Table 1) on muscovite from a mylonite, synkinematic to the low dip deformation planes of the mylonitic structures, constrains the minimum age of such tectonism and its relationship with the Mesoproterozoic activity (Campal et al., 1995; Gaucher et al., 1996).

The Cerro Villalba Formation of the Basal Group (Gaucher and Sprechmann, 1995) that crops out in the vicinity of the Minas village provides a complementary picture of the structural history of the Nico Perez domain. This formation that contains thick stromatolites and synsedimentary stromatolitic breccias was folded by two superposed events, in conjunction with the lower and upper formations (metaconglomerates, muscovitic schists and quartzites) of the stratigraphic sequence. Detailed stratigraphic studies (Gaucher et al., 1996) defined a marine, shallowing-upward environment for the Basal Group basin, evidenced by graded metaconglomerates intercalated with metapelites (interpreted as proximal turbidites) and the observed transitional contact between these lithologies and recrystallized shales (carbonate platform deposits) intercalated with thick limestones, at the base of the Cerro Villalba formation, passing into stromatolites (very shallow subtidal to intertidal environment). The Upper Quartzite formation was interpreted to represent very shallow transitional conditions or possibly continental sedimentation.

The first overprinting event in the Basal Group is represented by a N–S fabric and is considered to be coeval with 1250 Ma important thrusts (see above). It is overprinted by a N75E–S75W foliation. This is the only fabric observed in the Arroio del Soldado Group (560–545 Ma) — a passive continental margin sequence that overlies with angular unconformity the Basal Group (Campal et al., 1995; Gaucher and Sprechmann, 1995). Due to the diversity of the Cerro Villalba stromatolites [LLH-C, LLH-S, SH-V types; Logan et al. (1964)] and the structural relations with the overlaying Vendian sequence, a minimum Mesoproterozoic deposition age (ca 1600–1300 Ma) was proposed for the Basal Group (Campal et al., 1995; Gaucher and Sprechmann, 1995).

The Illescas rapakivi granite (Campal and Schipilov, 1995) crops out in the vicinity of Nico Perez and Illescas villages (Fig. 1) and yielded a Rb–Sr whole rock isochron age of 1760 ± 32 Ma and $Sr_0 = 0.704$ [Bossi and Campal (1992) re-calculated from Umpierre and Halpern (1971)]. This age has been recently confirmed by a 1751 Ma U–Pb age on zircon from this granite (L. Heaman, personal communication, 1994). Subsequently, the batholith was overprinted by shear zones trending N10W to N–S that are subparallel to the trend of the Sarand Del Yi fault. This led Campal et al. (1995) to interpret this tectonism as correlated with the oldest foliation recorded in the Cerro Villalba rocks (see above) and consider this fault active since the Mesoproterozoic time.

The Nico Perez domain was also affected by shear zones exhibiting tectonic vergence opposite to the 1250 Ma thrusts (see above). A mylonite within one of these shear zones yielded a K–Ar muscovite age of 572 ± 7 Ma, showing the genetic relationship with the Brazilian orogeny of eastern Uruguay (Bossi and Campal, 1992). In addition, younger granitic intrusions and mafic dikes within the domain yield ages in the 660–560 Ma range, and are similarly associated with this orogeny (Umpierre and Halpern, 1971; Mazzucchelli et al., 1995). Northward from the Nico Perez domain, in the Minas de Corrales-Vichadero and Aceguá regions (Fig. 1), gneisses of Transamazonian age were intruded by granites dated between 700 and 580 Ma (Cordani and Soliani, 1990).

3. The Uruguayan dike swarm

The UDS discordantly intrudes E–W mylonite zones related to the second deformational episode of the RLPC country rocks (Bossi and Campal, 1991). To the east, the swarm is truncated by the Sarandi Del Yi fault (Fig. 1). In the vicinity of this fault the dikes have been flexured (southward motion) and subjected to drag-folding, and coun-

try rocks were cataclastically and mylonitically deformed (Bossi and Navarro, 1988). Recent interpretation of gravity data indicates that this fault represents a major structure that separates the Nico Perez domain (see above) from the RLPC, as suggested by the reported well-defined pairs of NW trending positive–negative anomalies inferred in the Paleozoic Paraná basin located to the north of the Uruguayan shield (Hallinan et al., 1993).

The dikes are subparallel and subvertical. They show sharp contacts with the host rocks, most of them exhibiting chilled, aphyric, microcrystalline planar margins. These facts reveal that emplacement of the swarm occurred after the country rocks attained rigidity. The dikes trend ENE ca N70E, are >1000 m, reaching up to 26 km in length. Dike thicknesses range from 0.5 to 80 m. They are well exposed in quarries where the sampling was carried out.

Rb–Sr whole rock geochronology on several dikes of the swarm yielded an isochron of 1861 ± 125 Ma (2σ) with $Sr_0 = 0.7031 \pm 0.0012$ (MSWD = 1.29) interpreted to be the emplacement age of the UDS (Bossi et al., 1993). Two K–Ar determinations on biotites from granitic gneisses at the very contact with the dikes yielded 1828 ± 21 and 1786 ± 26 Ma (Table 1), and are similarly consistent to the Rb–Sr age above. However, eight K–Ar analyses carried out on plagioclase and whole rocks from the dikes yielded results between 1600 and 1170 Ma (Table 1). The wide range of the apparent ages suggests that these materials have been subjected to variable Ar loss since dike emplacement.

Geochemically, the dikes are classified as tholeiitic andesites and andesitic basalts (Bossi et al., 1993). The latter group predominates in the southernmost part of the swarm, whilst the tholleitic andesites appear to have preferential distribution within its northern part. The tholeiitic andesites have higher contents of TiO_2 and incompatible elements compared to the andesitic basalts and are the most evolved (Mg molar ratios between 0.40 and 0.56) compared to the least evolved andesitic basalts (0.25–0.31). Moreover, the chemical characteristics of the dikes coupled with their general enrichment in LILE and LREE and the Nd and Sr isotopic results (e.g. most data plot close to bulk earth values) led Bossi et al. (1993) to conclude that the UDS is ensialic and that metasomatism affected the mantle source subcontemporaneously with melting of the source rocks.

Field observations indicate that transverse fractures and faults may displace the andesitic (low TiO_2) basalt dikes sub-perpendicular to the strike, whereas the tholeiitic (high TiO_2) andesite dikes are not affected, indicating they are younger than the andesitic basalt dikes. However, the fact that the two dike groups are roughly parallel indicates that the regional crustal stress pattern was probably the same during emplacement of both groups (Campal and Garat, 1990). In addition, the geometric features of emplacement for both groups (e.g. progressive thinning, dike bifurcation, presence of subnormal displacements) indicate that the magma flow was subhorizontal, a result from fluid pressure under conditions of hydraulic fracturing (Bossi and Campal, 1991).

In general, the dikes are fresh, although secondary recrystallization of minerals may be present. Petrographically, they correspond to microgabbros of subophitic texture. In the tholeiitic andesites, plagioclase is An_{42}–An_{50}, pigeonite is scarce and augite, rarely zoned, is often mantled by green amphibole. Biotite and apatite are accessory phases. The andesitic basalts have more calcic plagioclase (An_{52}–An_{64}) and often zoned augite, sometimes accompanied by pigeonite. Magnetite and ilmenite and small quantities of pyrite and chalcopyrite are present in both dike types. Oxidation of titanomagnetite in both types resulted in maghemite, as inferred by thermomagnetic curves (D'Agrella Filho et al., 1997), but this is more common for the high TiO_2 tholeiitic andesites.

Coarse-grained, quartzofeldspathic interstitial intergrowths with either minor primary mica and/or amphibole, as well apatite occur in the interior of some dikes. K-feldspar and quartz are the primary components of these intergrowths that appear to be more abundant in the high TiO_2 dikes. They are herein termed 'micropegmatites' [following the criterion of Bossi and Campal (1991)] in order to distinguish them from felsic veins of granitic composition that may also be present at the dikes' margins. These felsic veins

are either rectilinear (2–10 cm thick), filling centrimetric fractures that extend transversely up to 2 m into the margins of the dikes, or may occur as irregular, thin patches over the dike's wall [see comments in Fig. 2(A and B)].

4. Sampling and experimental procedure

Sampling for ^{40}Ar–^{39}Ar and Rb–Sr geochronological studies was performed on medium- to coarse-grained rocks located in the interior of the tholeiitic andesite and andesitic basalt dikes, associated micropegmatites as well as felsic veins and country rocks. Fig. 1 shows the locations of the analyzed samples.

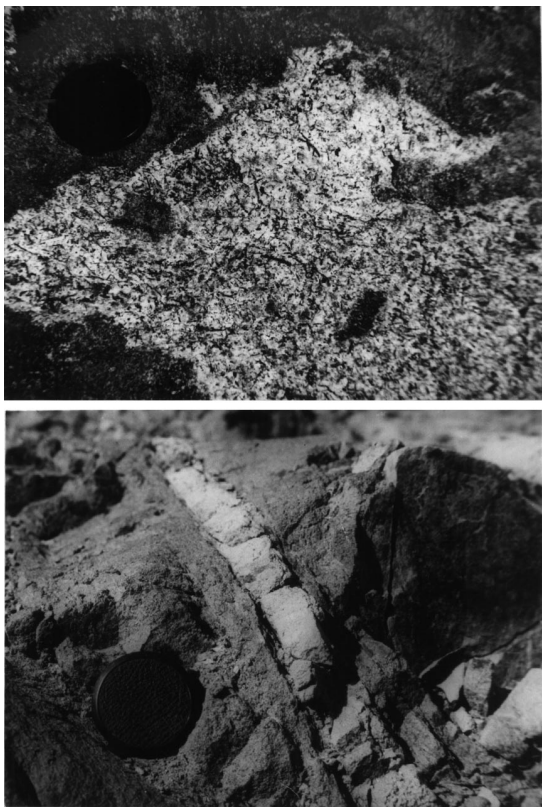

Fig. 2. Field aspects of the felsic veins that are present at the margins of some mafic dikes. (a) Irregular patch (light color) over the edge of the dike (dark); (b) rectilinear vein (light color) cutting the dike's wall (dark).

4.1. ^{40}Ar–^{39}Ar *method*

^{40}Ar–^{39}Ar analyses were performed at the Berkeley Geochronology Center, USA. Hornblende, biotite and muscovite were extracted from dike U-202 (high TiO_2 tholeiitic andesite) and two felsic veins (U-205, U-203), as well as three samples of the crystalline basement rocks. Samples were irradiated without Cd shielding for 49 h in the Omega West reactor at Los Alamos National Laboratory. The samples analysed were single crystals between 0.5 and 2.0 mm, except for U-202 hornblende which comprised 10 grains of 0.5 mm. Samples were degassed until fusion by incremental heating with a defocused Ar-ion laser for 30 s, followed by 150–210 s of gas purification with two SAES-172 getters, prior to analysis of each step. Laser control, valve actuation and mass spectroscopy were fully automated (Deino and Potts, 1990). Procedural background levels were measured between every three unknowns, and were similar to values reported by Deino and Potts (1990).

Given the large number of experiments performed, only a selection of the analytical data from the dikes is presented in Tables 2–9. Nevertheless, the complete data bank (dikes and country rocks) is available to the interested researchers upon request to the authors. Isotopic run data were corrected for mass discrimination, radioactive decay, and nucleogenic interferences. ^{40}Ar–^{39}Ar ages calculated herein are based on the age of Fish Canyon sanidine (27.84 Ma) as a fast neutron fluence monitor, whereas Renne et al. (1994, 1998) concluded that an age of 28.03 Ma is more appropriate for external comparison. We report ages herein relative to the younger value for comparison with previously published data, but note that the plateau age of 1727 Ma for the dike hornblende (see results below) recalculates to 1735 Ma if the older age (28.03 Ma) for the Fish Canyon sanidine is used.

The fluence parameter 'J' was determined from individual analysis of 15 sanidine grains in each of two positions bracketing (within 8 mm laterally, and 2 mm vertically) in the unknown samples. The two positions yielded indistinguishable results and then a weighted mean value of $J=0.03422\pm$

Table 2
^{40}Ar–^{39}Ar (selected steps) analytical data on the mafic dikes of the Uruguayan shield: U-202 Hornblende (5220-01)

Laser (W)	^{40}Ar (nA)	40/39	38/39	37/39	36/39	40*/39	% 40*	Age (Ma)	$\pm\sigma$ (Ma)
0.5	76.08	38.249	0.000	0.222	14.875	33.872	88.6	1388.5	9.2
0.7	78.96	46.107	0.079	0.248	1.281	45.753	99.2	1699.7	10.7
0.9	132.13	46.366	0.000	0.648	0.846	46.182	99.6	1710.0	10.4
1.1	330.52	47.166	0.490	2.387	0.985	47.128	99.8	1732.5	10.7
1.3	341.78	46.922	0.658	2.392	0.646	46.984	100.0	1729.1	10.7
1.5	340.86	46.848	0.696	2.635	1.026	46.823	99.8	1725.2	10.6
1.7	196.41	47.126	0.729	2.570	1.257	47.027	99.6	1730.1	11.0
1.9	199.42	46.755	0.676	2.732	0.723	46.830	100.0	1725.4	10.6
2.1	118.88	47.180	0.709	2.931	2.042	46.887	99.2	1726.8	12.2
2.3	12.22	46.104	0.469	2.128	0.822	46.084	99.8	1707.6	15.9
2.5	11.52	46.466	0.415	2.584	1.103	46.412	99.7	1715.5	14.8
2.7	169.15	45.700	0.658	4.449	1.150	45.829	100.0	1701.5	13.2

Table 3
^{40}Ar–^{39}Ar (selected steps) analytical data on the mafic dikes and country rocks of the Uruguayan shield: U-202 Biotite (5229-01)

Laser (W)	^{40}Ar (nA)	40/39	38/39	37/39	36/39	40*/39	% 40*	Age (Ma)	$\pm\sigma$ (Ma)
0.2	0.07	54.352	−0.164	0.000	−88.916	80.624	148.3	2388.7	718.9
0.3	153.87	39.882	0.058	0.016	18.711	34.352	86.1	1402.1	10.1
0.4	322.48	44.906	0.053	0.007	0.970	44.617	99.4	1672.1	10.7
0.8	441.89	47.084	0.058	0.004	0.076	47.059	100.0	1730.8	12.2
0.9	288.20	46.975	0.056	0.003	0.137	46.932	99.9	1727.8	10.7
1.1	171.56	46.678	0.057	0.003	0.183	46.622	99.9	1720.5	10.6
1.2	143.72	47.180	0.062	0.003	0.231	47.109	99.9	1732.0	10.6
1.3	120.72	46.839	0.070	0.003	0.224	46.771	99.9	1724.0	10.7
1.4	61.05	46.368	0.076	0.002	0.138	46.325	99.9	1713.4	13.3
1.6	28.27	46.908	0.070	0.004	0.940	46.629	99.4	1720.6	11.7
1.7	19.31	47.024	0.071	0.003	0.773	46.794	99.5	1724.5	12.0
2.0	19.27	46.519	0.062	0.004	0.245	46.445	99.8	1716.2	12.2
2.8	17.00	46.124	0.048	0.004	−0.137	46.163	100.1	1709.5	11.8
3.5	83.08	46.543	0.073	0.002	−0.181	46.594	100.1	1719.8	10.9
4.0	70.82	46.672	0.050	0.001	0.098	46.641	99.9	1720.9	10.9
5.0	161.44	47.148	0.049	0.002	0.141	47.104	99.9	1731.9	10.7

0.00031 was used for all samples. The uncertainty in this value does not include uncertainty in the age of the monitor.

Atmosphere-corrected data are plotted as apparent age spectra in Figs. 2–7. Each of the apparent age spectra is accompanied by compositional Ca/K (or K/Ca) and Cl/K data derived from corrected relative abundances of ^{37}Ar, ^{38}Ar and ^{39}Ar for each step. It should be noted that the Ca/K values are $1.96 \times {}^{37}Ar_{Ca}/{}^{39}Ar_{K}$, whereas the Cl/K values shown are actually values of $^{38}Ar_{Cl}/^{39}Ar_{K}$.

Apparent age plateaus are herein defined following Fleck et al. (1977), and plateau ages are calculated as the inverse variance weighted mean of all steps defining the plateau. Uncertainties on plateau ages (1σ) were determined by calculating the inverse variance weighted mean $^{40}Ar^{*}/^{39}Ar_{K}$ of the plateau steps, then applying quadratic error propagation to the age equation, following Renne et al. (1996). The latter approach was used because direct error propagation through the weighted mean age calculation results in errors (typically 0.1%) far smaller than the limiting systematic uncertainty (0.9%) in 'J' permits, and is clearly a

Table 4
^{40}Ar–^{39}Ar (selected steps) analytical data on the mafic dikes of the Uruguayan shield: U-202 Biotite (5229-02)

Laser (W)	^{40}Ar (nA)	40/39	38/39	37/39	36/39	40*/39	% 40*	Age (Ma)	$\pm\sigma$ (Ma)
0.3	34.79	105.66	0.106	NA	251.86	31.238	29.6	1311.5	24.4
0.4	6.22	53.303	0.072	NA	81.926	29.091	54.6	1246.3	15.1
0.5	2.05	37.476	0.067	NA	36.537	26.677	71.2	1170.0	20.8
0.5	1.46	36.784	0.076	NA	38.041	25.540	69.4	1133.0	17.3
0.6	1.13	31.663	0.073	NA	31.596	22.632	71.3	1034.5	21.1
0.6	1.13	26.873	0.075	NA	24.353	19.675	73.2	928.6	14.4
0.7	1.05	23.565	0.083	NA	17.322	18.444	78.3	882.6	14.1
0.7	1.09	19.584	0.079	NA	16.568	14.686	75.0	734.5	12.1
0.8	1.23	15.526	0.073	NA	9.865	12.609	81.2	647.0	8.8
0.8	1.39	13.795	0.073	NA	8.596	11.554	83.6	601.0	12.5
0.9	1.54	13.603	0.066	NA	8.610	11.153	81.9	583.1	15.4
0.9	1.81	14.185	0.067	NA	8.603	11.640	82.1	604.8	13.8
1.0	1.94	16.771	0.063	NA	10.042	13.801	82.3	697.7	13.5
1.0	1.92	22.043	0.068	NA	7.972	20.286	91.6	951.0	16.6
1.1	2.15	27.709	0.066	NA	7.689	25.435	91.8	1129.5	12.2
1.1	2.58	37.005	0.065	NA	7.985	34.643	93.6	1410.4	13.0
1.2	3.28	43.247	0.070	NA	12.483	39.556	91.5	1544.0	12.6
1.2	3.97	44.644	0.066	NA	9.261	41.945	93.9	1605.6	13.3
1.3	5.11	45.006	0.061	NA	8.578	42.469	94.4	1618.9	12.9
1.3	6.24	44.671	0.070	NA	8.172	42.253	94.6	1613.4	13.6
1.4	9.57	44.583	0.069	NA	8.558	42.052	94.3	1608.4	11.8
1.5	13.06	43.599	0.066	NA	7.183	41.474	95.1	1593.7	10.9
1.6	18.74	43.103	0.067	NA	5.988	41.422	96.0	1592.3	11.2
1.7	26.79	43.672	0.066	NA	5.600	42.015	96.2	1607.4	10.9
1.8	33.00	43.600	0.067	NA	3.770	42.483	97.4	1619.2	10.9
2.0	38.40	45.597	0.065	NA	1.641	45.110	98.9	1684.1	11.3
2.4	20.29	46.667	0.078	NA	0.485	46.522	99.7	1718.1	12.1
2.8	11.50	46.639	0.075	NA	0.457	46.508	99.7	1717.7	15.7
3.0	8.23	47.524	0.076	NA	0.860	47.267	99.5	1735.8	16.5
3.6	9.75	47.595	0.077	NA	0.742	47.418	99.6	1739.3	21.5
4.0	10.85	46.579	0.088	NA	0.543	46.434	99.7	1716.0	16.0
4.5	12.99	47.484	0.089	NA	1.344	47.151	99.3	1733.0	14.7
5.0	11.43	46.332	0.084	NA	0.370	46.308	99.9	1713.0	15.8
5.5	15.81	46.413	0.063	NA	0.231	46.342	99.9	1713.8	13.5
7.0	1.19	16.963	0.000	NA	6.479	15.152	89.3	753.5	11.2

more accurate estimation of the uncertainty in any $^{40}Ar/^{39}Ar$ plateau age.

4.2. Rb–Sr method

Rb–Sr determinations were carried out at the Geochronological Research Center-CPGeo, University of São Paulo, São Paulo, Brazil. The following outcrops were studied:

(1) andesitic basalts (low TiO_2): U-201 (Pichinango quarry) and U-205B (Iviil quarry);
(2) tholeiitic andesites (high TiO_2): U-202B (Brandal quarry), U-209B (Stonelux quarry) and U-216A (Monica quarry);
(3) felsic veins U-202A (intrusive into dike U-201) and U-205A (intrusive into dike U-205B).

Sample sizes varied from to 2 to 3 kg. Medium-grained dike material was selected for separation of 80–100 mesh mineral fractions and whole rock aliquot (WR) analyses. The concentrates correspond to progressively less magnetic fractions (indicated by F, M, M1, M3; see Figs. 10, 12 and 13), dependent on intensity of the magnetic field of the Frantz separator (typically operated at 1.0 to 0.3 amp). The fractions that include predomi-

Table 5
^{40}Ar–^{39}Ar (selected steps) analytical data on the mafic dikes of the Uruguayan shield: U-205 Muscovite (5227-01)

Laser (W)	^{40}Ar (nA)	40/39	38/39	37/39	36/39	40*/39	% 40*	Age (Ma)	$\pm\sigma$ (Ma)
0.3	2.26	45.488	0.109	0.029	38.978	33.971	74.7	1391.3	36.3
0.3	3.08	45.228	0.050	0.019	8.645	42.673	94.4	1624.0	22.9
0.4	7.32	45.982	0.022	0.005	1.168	45.635	99.2	1696.8	14.4
0.6	11.82	46.576	0.022	0.007	−0.320	46.669	100.2	1721.6	12.2
0.7	177.80	46.441	0.027	0.000	0.523	46.284	99.7	1712.4	10.5
0.8	221.28	46.673	0.020	0.000	0.240	46.599	99.8	1719.9	11.4
0.9	116.41	46.130	0.021	0.000	0.072	46.107	100.0	1708.2	10.8
1.0	196.97	46.325	0.022	0.000	0.040	46.311	100.0	1713.1	10.4
1.2	548.36	46.713	0.023	0.000	0.020	46.704	100.0	1722.4	10.9
1.3	274.72	46.297	0.021	0.000	0.024	46.288	100.0	1712.5	10.5
1.5	73.92	46.173	0.021	0.000	−0.142	46.213	100.1	1710.7	10.7
1.7	56.12	46.366	0.022	0.000	0.078	46.341	100.0	1713.8	12.6
2.7	15.34	46.709	0.020	0.002	0.322	46.611	99.8	1720.2	12.4
4.0	43.32	46.364	0.027	0.001	0.608	46.182	99.6	1710.0	10.9

Table 6
^{40}Ar–^{39}Ar (selected steps) analytical data on the mafic dikes of the Uruguayan shield: U-205 Biotite (5228-01)

Laser (W)	^{40}Ar (nA)	40/39	38/39	37/39	36/39	40*/39	% 40*	Age (Ma)	$\pm\sigma$ (Ma)
0.3	17.69	26.379	0.178	0.027	4.883	24.937	94.5	1113.0	8.8
0.3	52.86	32.830	0.182	0.018	1.581	32.362	98.6	1344.7	9.2
0.4	94.33	42.091	0.156	0.012	0.821	41.847	99.4	1603.2	10.2
0.4	106.81	44.072	0.161	0.012	0.689	43.867	99.5	1653.7	10.3
0.4	59.84	45.384	0.155	0.011	0.775	45.154	99.5	1685.2	11.0
0.5	81.30	45.684	0.158	0.010	0.420	45.559	99.7	1695.0	10.8
0.6	30.30	46.141	0.146	0.013	0.559	45.975	99.6	1705.0	11.5
0.7	23.23	46.081	0.147	0.013	0.826	45.836	99.5	1701.7	12.4
0.9	30.97	45.490	0.147	0.013	−0.257	45.565	100.2	1695.1	12.0
1.0	39.64	45.386	0.146	0.013	0.025	45.378	100.0	1690.6	10.8
1.2	50.19	45.274	0.154	0.014	0.510	45.123	99.7	1684.4	11.9
1.6	27.28	46.037	0.138	0.015	1.623	45.556	99.0	1694.9	13.3
2.0	60.75	46.344	0.126	0.012	0.889	46.080	99.4	1707.5	10.8

nantly felsic, less-magnetic minerals (mainly plagioclase) yielded lower Rb–Sr ratios than the ones with mafic, more magnetic minerals (olivine, pyroxene, amphibole, mica). A hand-magnet separation produced an additional, mostly magnetic fraction of each sample (magnetite, ilmenite-HM in Figs. 10, 12 and 13). The objective of obtaining concentrates of different magnetic susceptibility was to generate fractions with varying Rb–Sr values compared to the WR data and thus attain more precise ages. The felsic vein samples underwent a similar treatment.

The $^{87}Sr/^{86}Sr$ ratios were measured on unspiked samples using a VG-354 single collector mass spectrometer. These ratios were normalized to $^{86}Sr/^{88}Sr = 0.1194$, and the final quoted errors are external ones (1σ level) based on replicate analyses of $SrCO_3$ NBS-987 which yielded an average ratio of 0.71026 ± 0.00003 (1σ level) during the period of the analyses. The Rb and Sr contents were determined by X-ray fluorescence (XRF) with a 2.0% precision for each of these elements. Isotope dilution measurements of the Rb and Sr contents were performed in some of the samples (see

Table 7
^{40}Ar–^{39}Ar (selected steps) analytical data on the mafic dikes of the Uruguayan shield: U-203 Biotite (5626-01)

Laser (W)	^{40}Ar (nA)	40/39	38/39	37/39	36/39	40*/39	% 40	Age (Ma)	± (Ma)
0.3	333.89	35.304	0.049	0.006	4.667	33.923	96.1	1389.9	9.8
0.4	612.76	42.136	0.045	0.004	0.786	41.902	99.4	1604.6	10.4
0.4	960.99	44.978	0.044	0.003	0.417	44.853	99.7	1677.9	10.9
0.5	1171.24	46.690	0.046	0.003	0.302	46.599	99.8	1719.9	10.6
0.5	601.83	46.329	0.047	0.003	0.268	46.248	99.8	1711.6	10.9
0.6	372.69	46.263	0.047	0.004	0.392	46.145	99.7	1709.1	10.9
0.6	316.51	45.863	0.046	0.005	0.433	45.733	99.7	1699.2	10.7
0.7	153.94	45.239	0.046	0.010	0.613	45.056	99.6	1682.8	10.7
0.9	302.08	45.585	0.046	0.012	0.526	45.428	99.7	1691.8	10.6
1.0	240.17	44.999	0.047	0.014	0.534	44.840	99.7	1677.6	10.9
1.1	312.99	45.970	0.047	0.007	0.616	45.787	99.6	1700.5	11.4
1.5	91.22	44.118	0.048	0.006	0.138	44.076	99.9	1658.9	10.8
1.7	68.08	43.543	0.048	0.008	0.494	43.395	99.7	1642.0	10.6
2.3	23.68	44.816	0.049	0.012	0.622	44.631	99.6	1672.5	11.1
2.6	19.73	45.089	0.047	0.014	0.094	45.060	99.9	1682.9	11.1
3.5	11.23	45.530	0.047	0.013	0.017	45.524	100.0	1694.2	15.2
5.0	300.04	45.002	0.047	0.015	0.472	44.862	99.7	1678.1	10.4

Table 10) and the average precision (1σ level) for the calculated $^{87}Rb/^{86}Sr$ ratios is 1.40%. All decay constants are those recommended by Steiger and Jäger (1977). The overall blank for the chemical procedure was <6 ng for Sr.

The isochrons were fitted following the principles of Williamson (1968), in which the experimental variance was used to weight each point. The precision on the age and initial $^{87}Sr/^{86}Sr$ ratios are quoted at the 95% (2σ) confidence level. In addition, a best fit line was calculated in the case that whole rock data refer to different outcrops (Fig. 9), in order to minimize minor differences in the initial $^{87}Sr/^{86}Sr$ ratios that might exist for the dikes. These data regression, therefore, did not provide a MSWD value.

5. Results and discussion

5.1. ^{40}Ar–^{39}Ar *results*

5.1.1. *Country rocks*

Three country rock samples were analyzed (locations in Fig. 1) in order to help clarify the geologic history of the RLPC in the region of the UDS. The Pintos granodiorite is representative of intrusive granitoids emplaced after the Transamazonian metamorphism. The hornblende was degassed in 17 steps, yielding an integrated age of 2014 ± 13 Ma with a plateau age of 2016 ± 11 Ma [Fig. 3(A)]. A grain of biotite degassed in 28 steps yields an integrated age of 1813 ± 13 Ma, with a plateu age of 1817 ± 10 Ma [Fig. 3(B)]. The 200 Ma difference between the coexisting minerals implies very slow cooling ($\sim 1^{\circ}C\ Ma^{-1}$) between ~ 500 and $\sim 300^{\circ}C$ (Baldwin et al., 1990; Harrison et al., 1985), or preferential Ar loss from the biotite during subsequent reheating. The presence of magmatic epidote in this granitoid suggests a mid- to deep crustal emplacement depth (Zen and Hammarstrom, 1984), consistent with the favored interpretation of slow cooling.

Biotite from another granitoid (U-206E), collected ~ 50 m from the contact with the dike represented by sample U-206A, was degassed in 29 steps, yielding an integrated age of 1913 ± 14 Ma and a plateau age of 1916 ± 11 Ma [Fig. 3(C)]. This age is significantly older than the biotite plateau age of the Pintos granodiorite cited above, and suggests the existence of distinct plutonic pulses within the RLPC. As with both the Pintos biotite and hornblende, the spectrum is slightly disturbed with anomalously young apparent ages for the low temperature steps. The discor-

Table 8
^{40}Ar–^{39}Ar (selected steps) analytical data on the mafic dikes of the Uruguayan shield: U-203 Biotite (5226-02): part 1

Laser (W)	^{40}Ar (nA)	40/39	38/39	37/39	36/39	40*/39	% 40*	Age (Ma)	$\pm\sigma$ (Ma)
0.3	2.14	55.173	0.067	NA	92.447	28.261	51.1	1220.4	20.1
0.4	0.72	39.508	0.048	NA	35.091	29.136	73.8	1247.7	21.2
0.5	0.55	38.322	0.054	NA	30.137	29.414	76.8	1256.2	36.9
0.5	0.59	36.701	0.047	NA	26.278	28.934	78.8	1241.4	24.9
0.6	0.74	37.513	0.043	NA	29.664	28.745	76.6	1235.6	27.4
0.6	0.74	34.641	0.046	NA	21.865	28.178	81.3	1217.8	18.8
0.7	0.82	35.514	0.049	NA	24.319	28.729	80.7	1235.0	22.2
0.7	1.28	33.417	0.049	NA	16.927	28.412	85.0	1225.2	14.5
0.8	1.24	31.885	0.052	NA	14.142	27.704	86.9	1202.9	18.3
0.8	1.56	34.059	0.052	NA	22.075	27.534	80.8	1197.5	18.3
0.9	1.44	29.626	0.047	NA	8.390	27.144	91.6	1185.0	12.2
0.9	1.56	29.713	0.050	NA	7.731	27.426	92.3	1194.0	15.6
1.0	1.83	29.764	0.050	NA	8.607	27.218	91.5	1187.4	11.5
1.0	1.70	30.555	0.041	NA	4.304	29.281	95.8	1252.1	10.3
1.1	2.29	31.753	0.046	NA	5.655	30.079	94.7	1276.6	10.0
1.1	2.65	32.213	0.044	NA	4.317	31.031	96.3	1305.3	10.4
1.2	3.02	33.572	0.047	NA	3.968	32.397	96.5	1345.8	10.5
1.2	3.63	35.067	0.046	NA	3.871	33.921	96.7	1389.8	10.2
1.3	5.56	36.234	0.044	NA	3.036	35.334	97.5	1429.8	10.4
1.4	7.80	37.795	0.045	NA	2.765	36.976	97.8	1475.1	10.5
1.5	12.23	38.740	0.045	NA	2.411	38.043	98.2	1503.9	11.2
1.6	17.23	40.500	0.046	NA	1.962	39.933	98.6	1553.9	10.9
1.7	22.88	41.318	0.046	NA	1.836	40.863	98.8	1578.0	10.5
1.8	24.11	42.111	0.045	NA	1.422	41.689	99.0	1599.1	10.8
1.9	31.96	42.590	0.045	NA	1.160	42.247	99.2	1613.3	10.3
1.9	35.30	43.276	0.045	NA	1.186	42.923	99.2	1630.3	10.6
2.0	37.29	43.415	0.045	NA	0.941	43.162	99.4	1636.2	10.7
2.1	40.81	44.124	0.044	NA	0.861	43.875	99.4	1653.9	11.2
2.2	43.50	44.227	0.045	NA	0.730	44.009	99.5	1657.2	11.7
2.2	48.80	45.016	0.045	NA	0.461	44.878	99.7	1678.5	11.7
2.3	47.13	45.494	0.045	NA	0.629	45.315	99.6	1689.1	11.6
2.5	68.99	45.036	0.044	NA	0.491	44.897	99.7	1679.0	11.0
2.7	72.68	46.181	0.043	NA	0.498	46.031	99.7	1706.4	11.0
3.0	51.69	46.569	0.043	NA	0.532	46.409	99.7	1715.4	11.3

dant steps in the hornblende and biotite may correlate with minor alteration or inclusions, as compositional variations are indicated by Ca/K and Cl/K values.

An intrusive granodiorite occurring in the Nico Perez domain, representing one of the plutons related to the adjacent Brazilian orogeny of eastern Uruguay (e.g. Umpierre and Halpern, 1971), was also investigated. Hornblende from this pluton (U-222A) was degassed in 13 steps, yielding an integrated age of 606 ± 6 Ma and a plateau (defined by the last three steps) of 596 ± 5 Ma [Fig. 4(A)]. The lowest temperature discordance associated with low Ca/K and Cl/K is probably due to phyllosilicate alteration, as observed in the experiments performed on the RLPC granitoids (see above). The apparent ages for hornblende U-222A decrease down to the plateau in a manner suggestive of extraneous Ar. The last five steps have relatively uniform Ca/K and Cl/K values devoid of chemical anomalies, and the resulting errorchron yields 580 ± 5 Ma with initial $^{40}Ar/^{36}Ar = 920 \pm 23$ and MSWD = 39.5 (not shown). Thus the presence of extraneous Ar is suggested (although the scattered data suggest multiple components of nonradiogenic argon), and the Ar retention age of this sample is best estimated at 580 ± 5 Ma.

Table 9
^{40}Ar–^{39}Ar (selected steps) analytical data on the mafic dikes of the Uruguayan shield: U-203 Biotite (5226-02): part 2

Laser (W)	^{40}Ar (nA)	40/39	38/39	37/39	36/39	40*/39	% 40*	Age (Ma)	$\pm\sigma$ (Ma)
3.0	44.57	45.930	0.044	NA	0.058	45.911	100.0	1703.5	12.0
3.2	31.79	45.977	0.043	NA	0.441	45.844	99.7	1701.9	11.9
3.3	27.43	45.801	0.044	NA	0.398	45.681	99.7	1697.9	12.8
3.3	22.88	46.289	0.046	NA	0.294	46.309	100.0	1713.0	13.9
3.5	18.21	46.383	0.044	NA	0.573	46.286	99.8	1712.5	13.5
3.5	16.44	45.306	0.043	NA	0.260	45.227	99.8	1687.0	15.0
3.6	14.45	45.684	0.041	NA	0.340	45.660	99.9	1697.4	14.3
3.8	11.34	44.542	0.039	NA	0.044	44.527	100.0	1669.9	14.6
3.8	11.34	44.165	0.040	NA	−0.085	44.223	100.1	1662.5	13.7
3.9	10.46	45.443	0.043	NA	−0.094	45.468	100.1	1692.8	20.0
4.0	9.39	46.060	0.042	NA	−0.007	46.060	100.0	1707.0	19.5
4.1	9.36	45.871	0.034	NA	0.993	45.575	99.4	1695.4	28.4
4.3	11.92	44.161	0.041	NA	0.500	44.011	99.7	1657.3	15.8
4.5	12.90	44.346	0.042	NA	0.505	44.194	99.7	1661.8	13.3
4.7	13.81	44.927	0.041	NA	0.521	44.911	99.9	1679.3	13.9
4.9	14.29	45.426	0.042	NA	0.122	45.388	99.9	1690.9	13.8
5.1	16.21	44.501	0.043	NA	0.194	44.441	99.9	1667.8	14.3
5.3	36.37	44.415	0.043	NA	0.754	44.211	99.5	1662.2	11.6
5.4	27.04	43.647	0.043	NA	0.657	43.451	99.6	1643.4	12.8
5.6	20.75	44.420	0.041	NA	0.485	44.274	99.7	1663.7	12.2
2.0	125.49	44.984	0.043	NA	0.476	44.843	99.7	1677.6	10.9
2.2	69.48	44.938	0.041	NA	0.343	44.871	99.8	1678.3	10.6
2.4	44.78	44.021	0.041	NA	0.524	43.916	99.7	1654.9	12.3
2.5	41.04	45.183	0.043	NA	0.423	45.089	99.8	1683.6	12.5
2.7	25.98	45.115	0.040	NA	0.462	44.976	99.7	1680.9	13.0
3.0	24.85	45.802	0.045	NA	0.561	45.667	99.7	1697.6	12.8
3.2	25.61	44.818	0.044	NA	0.400	44.771	99.9	1675.9	12.5
3.6	21.68	45.341	0.043	NA	0.406	45.253	99.8	1687.6	13.7
4.2	18.89	45.608	0.045	NA	0.573	45.436	99.6	1692.0	12.3
4.9	10.59	46.859	0.045	NA	0.117	46.828	99.9	1725.4	15.6
7.0	66.30	44.528	0.042	NA	1.644	44.049	98.9	1658.2	15.8

Biotite from the same sample (U-222B) was degassed in 25 steps, yielding an integrated age of 562 ± 5 Ma and a plateau age of 563 ± 4 Ma [Fig. 4(B)]. This biotite shows only minor internal discordance compared with the other biotites analyzed in this study, and is relatively undisturbed. Comparatively small discordance between the hornblende and biotite suggests moderately rapid cooling between 500 and 300°C after granitoid emplacement within the Nico Perez domain.

5.1.2. Mafic dikes

Igneous biotite and hornblende were extracted from a micropegmatitic intergrowth in the low TiO_2 dike U-202 (site 2; Fig. 1). The hornblende was degassed in 12 steps yielding an integrated age of 1708 ± 12 Ma and a plateau age of 1727 ± 10 Ma [Fig. 5(A)]. Discordance of the three lowest temperature fractions is probably correlated with cryptic intergrowth of a low Ca/K and Cl/K phase such as biotite. Two grains of biotite from this sample were analyzed individually. The first (U-202 Biotite-1) degassed in 22 steps (16 shown in Table 3), yields an integrated age of 1709 ± 13 Ma and a plateau age of 1725 ± 10 Ma [Fig. 5(B)]. Low temperature discordance (first two steps) in this case shows a slight correspondence with low K/Ca (although the variation is much smaller than in the case of the basement biotites). Either Ar loss or the growth of secondary phases (not observed petrographically) are suggested by the discordance. The concordance of

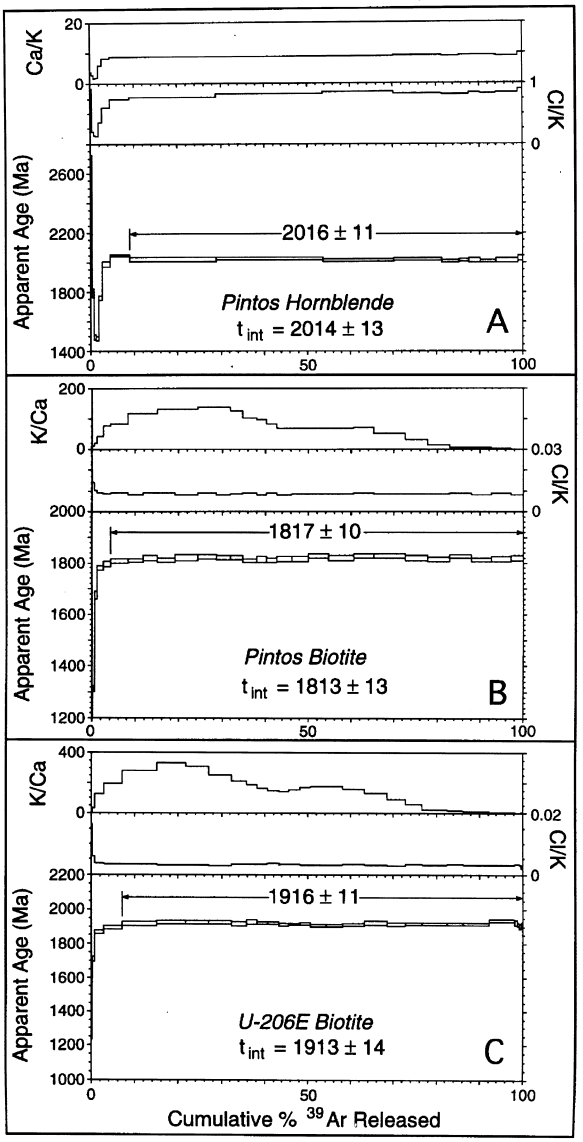

Fig. 3. ^{40}Ar–^{39}Ar spectra for country rocks in the area of the UDS: (A) hornblende and (B) biotite from the Pintos granodiorite; (C) granitoid collected ca 50 m from the contact with dike U-206.

plateau ages of both hornblende and biotite from dike U-202 suggests that the dike cooled rapidly and thus the crystallization age is taken as 1727 ± 10 Ma (the hornblende age).

It is noteworthy, however, that the first step obtained for both hornblende and biotite is

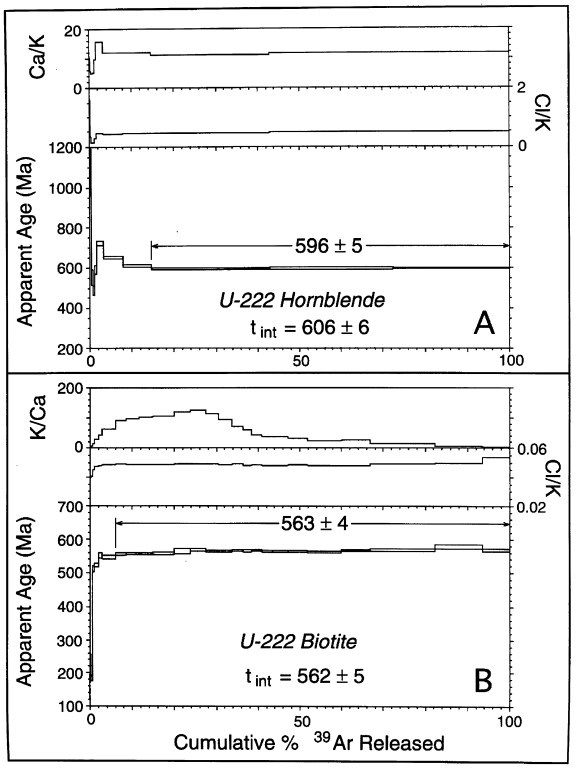

Fig. 4. ^{40}Ar–^{39}Ar spectra for (A) hornblende and (B) biotite from a granodiorite in the Nico Perez domain.

~1400 Ma. If the discordance was due to episodic Ar loss, a younger episode probably caused such a partial degassing, as illustrated in the thermochronology of the Imataca granulitic complex in Venezuela (e.g. Onstott et al., 1989).

In order to elucidate the significance of low temperature discordance in the biotite, a second grain (U-202 Biotite-2) was degassed in 52 steps (34 listed in Table 4). A similar integrated age (1697 ± 14 Ma) and plateau age (1728 ± 10 Ma) were obtained [Fig. 6(A)], but the detailed structure of the low temperature portion of the spectrum is more clearly defined by the first 4% released of the ^{39}Ar in 22 steps [Fig. 6(B)]. Fig. 5(B) shows that this initial 4% of the ^{39}Ar yields a saddle shaped pattern, with an apparent age minimum at ~600 Ma. Steps 3–11 define a linear array on an isotope correlation diagram [Fig. 6(C)], interpreted as a binary mixture of radiogenic Ar whose isochron age is 421 ± 14 Ma

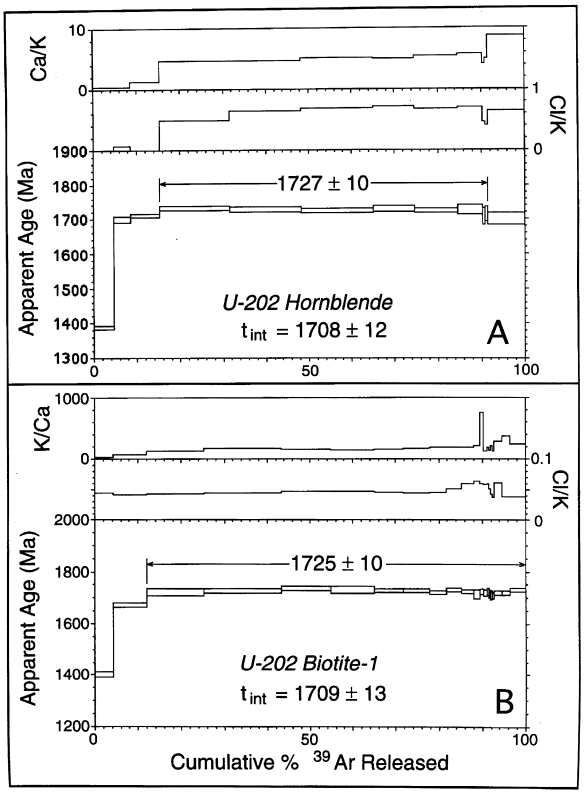

Fig. 5. ^{40}Ar–^{39}Ar spectra for (A) hornblende and (B) biotite from micropegmatitic intergrowth in dike U-202.

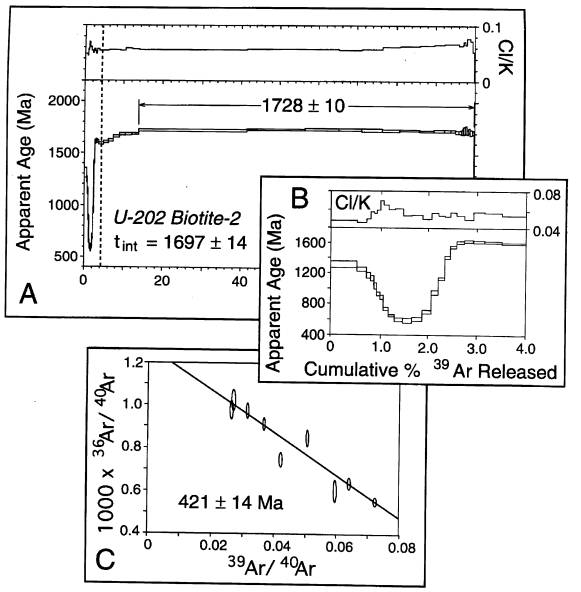

Fig. 6. (A) ^{40}Ar–^{39}Ar spectrum for biotite-2 from dike U-202; (B) detail of low temperature portion of the spectrum; (C) isotope correlation diagram for the steps shown in (B).

with an extraneous component having initial $^{40}Ar/^{36}Ar = 794 \pm 21$ ($N = 9$, MSWD = 2.07).

U-202 Biotite-2 was analyzed 13 months after irradiation so that Ca/K values could not be obtained due to radioactive decay of ^{37}Ar. The $^{38}Ar_{Cl}/^{39}Ar_K$ values for the discordant interval show minor enrichment in the steps yielding the younger age, but only by $<20\%$ compared to values in the plateau. This enrichment may be associated with the extraneous Ar component or with compositional zonation in the biotite; association with cryptic alteration and/or inclusions cannot be excluded but is thought to be less likely in view of detailed petrographic examination and careful selection of single grains.

Our preferred conclusion is that the apparent age spectrum reflects either very minor episodic outgassing or alteration of the biotite at 421 ± 14 Ma in the presence of a fluid phase which introduced Cl and extraneous Ar into low retentivity crystal-chemical sites. Such an episode probably never exceeded $\sim 300°C$, the approximate closure temperature for Ar loss from biotite (Harrison et al., 1985). In any case, the reproducibility of the ^{40}Ar–^{39}Ar 'overprint' age in sequential steps (after accounting for extraneous Ar) suggests that the age has geological significance and it is not a composite result of gas from heterogeneous sources as would be the case with an episodically induced diffusion gradient.

5.1.3. Felsic veins

Two felsic veins were investigated. Muscovite from vein U-205A (site 5, Fig. 1) was degassed in 25 steps (14 shown in Table 5) yielding an integrated age of 1715 ± 13 Ma and a plateau age of 1713 ± 10 Ma [Fig. 7(A)]. Biotite from the same sample was degassed in 21 steps (13 shown in Table 6), yielding a strongly discordant spectrum with an integrated age of 1634 ± 13 Ma and a plateau age of 1700 ± 10 Ma [Fig. 7(B)]. The discordance of the biotite age spectrum is accompanied by slightly elevated Cl/K and Ca/K, which could reflect the presence of cryptic secondary

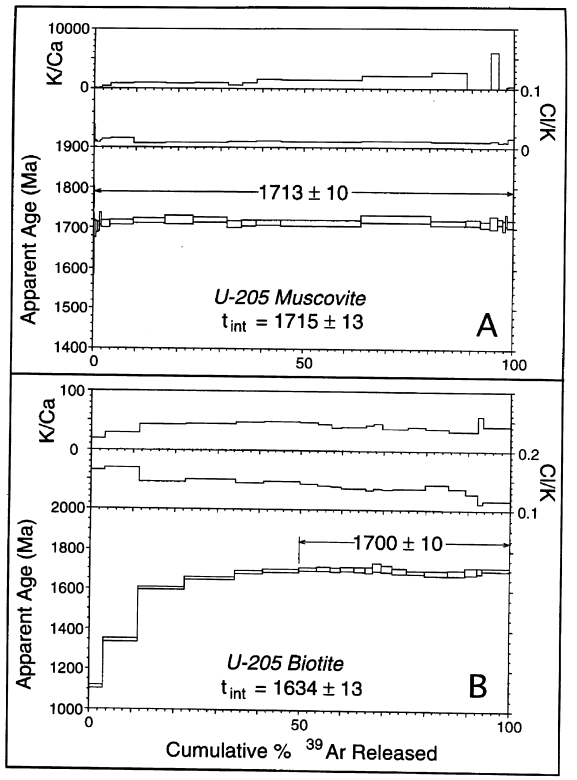

Fig. 7. ^{40}Ar–^{39}Ar spectra for (A) muscovite and (B) biotite from felsic vein intruding dike U-205.

phases. If interpreted as resulting from episodic Ar loss, the spectrum would indicate significant loss at ~1000 Ma, and the 1700 Ma plateau age could be significantly younger than the original Ar retention age of the biotite.

In any case, neither the muscovite or biotite plateau ages (1713±10 and 1700±10 Ma, respectively) for felsic vein U-205A are distinguishable at the 95% confidence level from the age (1727±10 Ma) inferred for the only dike dated directly, tholeiitic basalt U-202. The felsic vein U-205A clearly cuts the andesitic basalt dike U-205B (e.g. Fig. 3); however, based on the ^{40}Ar–^{39}Ar data available for dike U-202B the most straightforward conclusion is that the mafic dikes and felsic veins are approximately contemporaneous.

Biotite from another felsic vein, U-203 Biotite-1 was degassed in 22 steps (17 listed in Table 7) resulting in a strongly discordant spectrum [Fig. 8(A)] with no plateau, and an integrated age of 1667±13 Ma. The spectrum climbs monotonically for the first four steps to a maximum apparent age of 1720±11 Ma, then decreases and becomes somewhat erratic. Curiously, the first step is again ~1400 Ma, and an event of Ar loss younger than this age — and similar to those interpreted from the other samples except U-202 Biotite-2 — could be inferred from the data.

To investigate the significance of the low temperature discordance, a second grain (U-203 Biotite-2) was degassed in 101 steps, 75 of which are presented in Tables 8 and 9 [Fig. 8(B)]. The resulting spectrum is again strongly discordant, with an identical integrated age (1668±15 Ma) and similar maximum age of 1715±11 Ma, which occurs at ~50% of the cumulative ^{39}Ar released. The first 2% of ^{39}Ar was released in 19 steps [Fig. 8(C)], with a pseudo-plateau (weighted mean of step ages) of 1205±7 Ma defined by the first 13 steps. All but the first of these steps yields a highly correlated array on an isotope correlation diagram [Fig. 8(D)], and linear regression of these data yields an isochron of 1169±13 Ma, with initial $^{40}Ar/^{36}Ar = 376 \pm 19$ ($N=12$, MSWD = 0.40). As with U-202 Biotite-2, this sample was analyzed too long after irradiation to enable measurement of ^{37}Ar, thus Ca/K cannot be used to help infer the cause of discordance. Cl/K values in the detailed spectrum do not differ significantly from the rest of the spectrum. We therefore conclude that the initial thirteen steps are attributable to the biotite and register the age of a secondary, low thermal overprint, which may have produced either slight recrystallization or episodic Ar loss.

5.2. Rb–Sr results

Rb–Sr geochronology on whole rock and mineral concentrates was carried out on five mafic dikes and two felsic veins (Table 10). Whole rock analyses of four mafic dikes were plotted together with 13 analyses available from several outcrops of the UDS (Bossi et al., 1993). Only two samples of high TiO_2 dikes (U-216A and U-209B) clearly do not belong to the linear array (Fig. 9) and demonstrate that either the Rb or Sr in these

Table 10
Rb–Sr analytical data for the dikes

Sample	Material	Rb (ppm)	Sr (ppm)	$^{87}Rb/^{86}Sr$	$^{87}Sr/^{86}Sr$
U-205B-2	M2	61.6	209.0	0.854±0.024	0.72036±0.00006
U-205B-4	L C	47.32[a]	290.08[a]	0.4725±0.0066	0.71666±0.00009
U-205B-5	M	75.62[a]	170.75[a]	1.284±0.018	0.72313±0.00006
U205A-1	B	632.39[a]	31.87[a]	64.57±0.89	1.97913±0.00022
U-205A-A	HM	457.8	57.6	24.12±0.56	1.19934±0.00008
U-205A-B	WR	151.2	195.3	2.253±0.063	0.76408±0.00021
U-205A-C	L C	168.2	219.1	2.234±0.063	0.76146±0.00006
U-205A-D	M	167.1	152.3	3.198±0.090	0.77977±0.00007
U-202A	HM	64.7	158.1	1.189±0.033	0.74482±0.00006
U-202A-B	WR	68.8	239.7	0.832±0.023	0.72607±0.00007
U-202A-D	M3	82.1	320.2	0.743±0.021	0.72326±0.00007
U-202A-E	L C	67.5	387.2	0.505±0.014	0.71724±0.00006
U-202B-A	HM	62.2	110.3	1.637±0.046	0.73724±0.00005
U-202B-B	WR	54.6	219.2	0.722±0.020	0.72302±0.00009
U-202B-C	M1	61.0	80.1	2.213±0.062	0.74921±0.00014
U-202B-D	M2	43.12[a]	99.60[a]	1.256±0.018	0.73857±0.00005
U/202B-E	M3	94.7	329.4	0.833±0.024	0.72372±0.00008
U-202B-F	L C	92.7	412.9	0.650±0.018	0.71600±0.00005
U-216A(A)	HM	40.03[a]	39.97[a]	2.918±0.040	0.76733±0.00007
U-216A(B)	WR	15.65[a]	147.62[a]	0.3074±0.0043	0.72431±0.00006
U-216A(C)	M1	62.7	106.1	1.718±0.048	0.75198±0.00010
U-216A(E)	M3	102.7	291.0	1.023±0.029	0.72628±0.00010
U-216A(F)	L C	52.7	384.3	0.397±0.011	0.71531±0.00009
U-209B-1	L C	102.0	363.8	0.813±0.023	0.72352±0.00009
U-209B-3	M2	75.0	236.7	0.919±0.026	0.72572±0.00013
U-209B-4	M1	56.0	231.0	0.703±0.020	0.72531±0.00010
U-209B-5	HM	90.9	216.9	1.215±0.034	0.72898±0.00009
U-209B-6	WR	101.7	235.5	1.252±0.035	0.72515±0.00014
U-201A	HM	50.93[a]	117.41[a]	1.259±0.018	0.73930±0.00006
U-201B	WR	20.93[a]	187.72[a]	0.3229±0.0045	0.71351±0.00006
U-201D	M1	22.71[a]	66.67[a]	0.988±0.014	0.72976±0.00008
U-201E	M3	43.38[a]	233.36[a]	0.5386±0.0075	0.71821±0.00005
U-201F	L C	17.97[a]	307.13[a]	0.1694±0.0023	0.70845±0.00007

[a]Rb–Sr contents determined by isotope dilution.

particular systems has been disturbed. It is noteworthy, however, that high TiO_2 U-202B and low TiO_2 U-201 dikes were not disturbed.

Fifteen samples define a best fit line with a slope corresponding to an age of 1766±124 Ma and $Sr_0=0.70512\pm0.00036$ (Fig. 9). This data regression was preferred to that of Williamson (1968) because these data incorporate different errors from the Rb and Sr determinations; the analyses reported in Bossi et al. (1993) have errors for the $^{87}Rb/^{86}Sr$ ratios of 7.1% compared to errors of 1.40% (isotope dilution) and 2.8% (from XRF) for the ratios measured at the CPGeo.

The 1766±124 Ma age agrees within error with the 1861±125 Ma age defined by Bossi et al. (1993), but a slightly higher Sr_0 is now indicated by the $^{87}Rb/^{86}Sr$ ratio of sample U-201B, which has the lowest value among the whole rocks in Fig. 9. The calculated $^{87}Sr/^{86}Sr$ values for $t_0=1.73$ Ga ($^{40}Ar/^{39}Ar$ age) range from 0.7034 to 0.7055 (Table 11). The low TiO_2 dikes have $^{87}Sr/^{86}Sr$ t_0 values between 0.7035 and 0.7044 (mean 0.7040), except for the U-201 dike (0.7055; see further discussion), whilst the high TiO_2 dikes have values between 0.7039 and 0.7051 (mean 0.7046). The distinct $^{87}Sr/^{86}Sr$ t_0 mean values

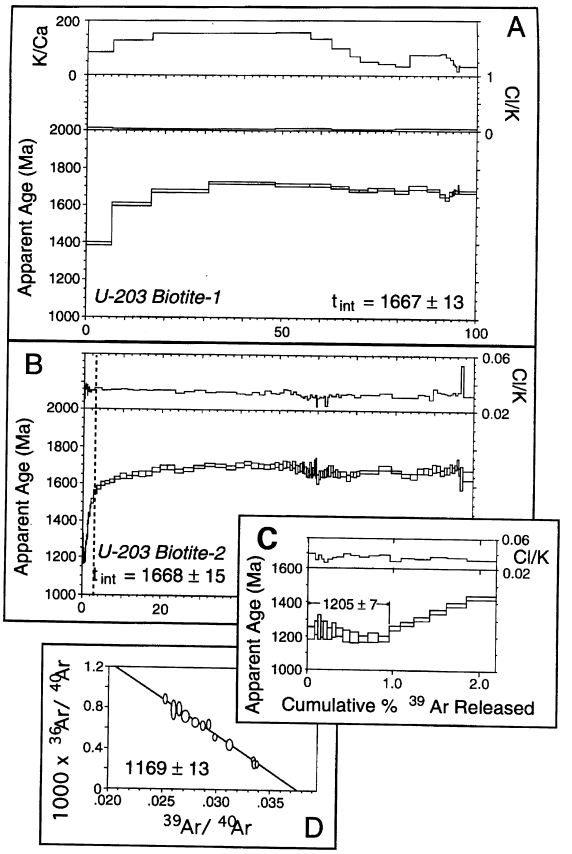

Fig. 8. (A) ^{40}Ar–^{39}Ar spectrum for biotite from felsic vein intruding dike U-203; (B) detailed spectrum (101 steps) for a second biotite grain from this vein; (C) inset showing the initial steps for grain depicted in (B); (D) isotope correlation diagram for the steps shown in (C).

among these dike groups are in agreement with the presence of two compositional different magmas, as supported by chemical inferences (Bossi et al., 1993). Nevertheless, the limited range in these values (see Table 11) is not compatible with the possibility of important crustal contamination by radiogenic ^{87}Sr. This all suggests that Rb and Sr have not been reset at the whole rock scale in most of the samples investigated since the emplacement of the UDS.

The mineral concentrates (F, M3, M1, HM) and whole rock from a micropegmatitic intergrowth that contains primary, accessory biotite and hornblende was sampled in the center of dike U-201 (30 m wide; low TiO_2 andesitic basalt). These materials yielded an errorchron age of 1900 ± 22 Ma with $Sr_0 = 0.7040 \pm 0.0011$ and MWSD = 16.0 (Fig. 10). This age is surprisingly old since a syntectonic granitoid located in the vicinity of this dike (Fig. 1; site '*f*') yielded a muscovite K–Ar cooling age of 1930 Ma (Ferrando and Fernandez, 1971). Also, it is inconsistent with the sharp chilled margin observed between dike U-201 and its host rock that demonstrates the crust had cooled prior to dike intrusion. A tentative cause for such an old age may lie in the presence of traces of primary biotite within the HM fraction that could possibly introduce a higher Sr_0 as compared to the other samples analyzed. If correct, this could explain the anomalous data plot of the HM fraction (Fig. 10). Nevertheless, taking into account the field relations (see Section 5.1) it is clear that the low TiO_2 andesitic basalts (e.g. U-201) are slightly older than the high TiO_2 tholeiitic andesites (e.g., U-202) for which a 1727 Ma ^{40}Ar–^{39}Ar age were obtained, as already seen.

Mineral concentrates and whole rocks from four other mafic dikes were analyzed in an attempt to investigate the thermal history of the swarm. The mineral concentrates showed very large scatter in the Rb–Sr diagram (Fig. 11) and best fit lines calculated for each dike (not shown herein) yielded a wide range of Rb–Sr dates that cover a larger span of time than the K–Ar apparent ages of the UDS (see Table 1): ca 1400 (U-216A); 1200 (U-202B); 960 (209B) and 570 Ma (U-205B). When all the data on mineral concentrates were plotted together, the result was a meaningless date of 1543 ± 163 Ma with $Sr_0 = 0.70504 \pm 0.07671$ (not shown in Fig. 11). The large data scatter compared to the plot of the 1766 Ma reference line (see above) indicates that the mineral systems have not remained closed to Rb and/or Sr after rock crystallization and raises the problem of whether one or more events overprinted the area. Indeed, the presence of uralite, accessory biotite, and maghemite in most of the dikes suggests the possibility that hydrothermal processes disturbed the Rb–Sr system.

Additional inferences for secondary Rb–Sr effects are provided by two felsic veins that are present at the margins of some mafic dikes. Felsic

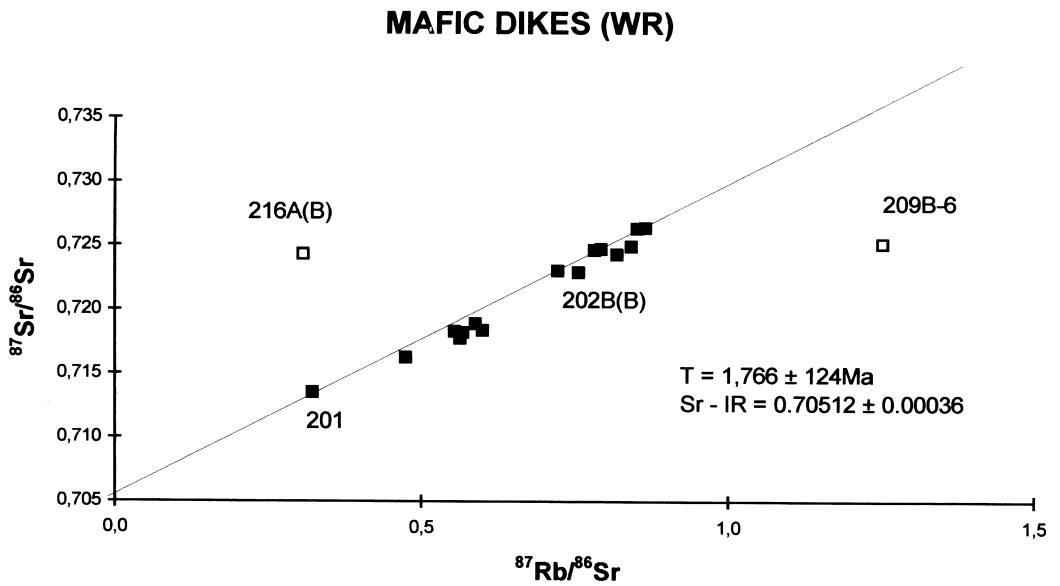

Fig. 9. Fifteen-point fit line on whole rocks. ■, Study samples + published analyses (Bossi et al., 1993); □, samples that were not considered in the regression.

Table 11
Recalculated $^{87}Sr/^{86}Sr$ initial ratios for $t_0 = 1.73$ Ga (see text for details)

Sample	Sr t_0
UR-1[a]	0.7041
UR-24[a]	0.7042
UR-42[a]	0.7045
UR-28[a]	0.7035
UR-10[a]	0.7037
UR-33[a]	0.7044
U-201B[a]	0.7055
UR-13[b]	0.7039
UR-30[b]	0.7052
U-202B-B[b]	0.7051
UR-4[b]	0.7041
UR-23[b]	0.7040
UR-16[b]	0.7050
UR-49[b]	0.7051
UR-58[b]	0.7049

Observations: UR samples (Bossi et al., 1993). Table 10 presents the analytical data of studied samples.
[a]Low TiO_2 dikes.
[b]High TiO_2 dikes, see text for details.

vein U-205A yields a five-point isochron of 1366 ± 18 Ma and MSWD = 0.95 (Fig. 12). The low MSWD value and the extremely high $^{87}Rb/^{86}Sr$ ratio of the biotite (64.57; Table 10) indicates that the isochron age is geologically significant. The high $Sr_0 = 0.7185 \pm 0.0010$ points that the minerals exchanged radiogenic ^{87}Sr until they all acquired the same $^{87}Sr/^{86}Sr$ ratio as the whole rock at the end of isotopic resetting.

It is noteworthy that ^{40}Ar–^{39}Ar plateau ages on muscovite (1713 Ma) and biotite (1710 Ma) herein presented constrain the emplacement age for the U-205 vein. The 1370 Ma Rb–Sr age obtained for this vein therefore records the timing of a thermal overprint in the UDS. Based on the ^{40}Ar–^{39}Ar data from felsic vein U-205, this event must not have exceeded 300°C (Harrison et al., 1985) because the muscovite spectrum is quite homogeneous whilst biotite is strongly discordant one [see Fig. 7(A and B)]. This interpretation agrees with the ^{40}Ar–^{39}Ar low temperature pattern for felsic vein U-203 (see Fig. 8). If, in fact, the felsic veins were reset, then the UDS mafic dikes have also been isotopically disturbed, as suggested by the geochronologic evidence in Figs. 5(A and B) and 6(B and C).

Finally, Rb–Sr analyses of felsic vein U-202A yielded a meaningless age older than the ^{40}Ar–^{39}Ar age of dike 202 whose margin it intrudes

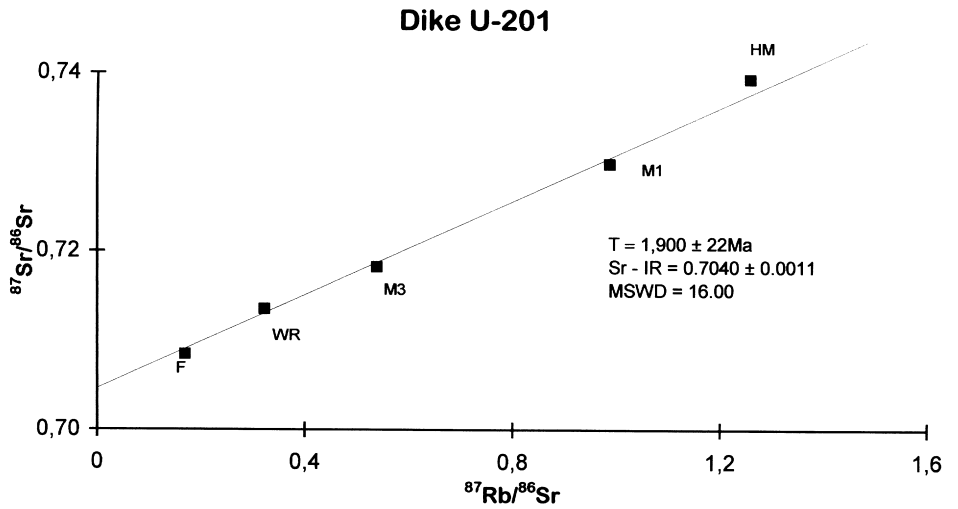

Fig. 10. Five-point errorchron; dike U-201. HM, Hand magnet fraction; M1, mafic, magnetic Frantz concentrate (>0.5 A); M3, mafic, magnetic Frantz concentrate (>1.0 A); F, felsic, less magnetic (<1.0 A) Frantz concentrate. WR, Whole rock. See text for explanation.

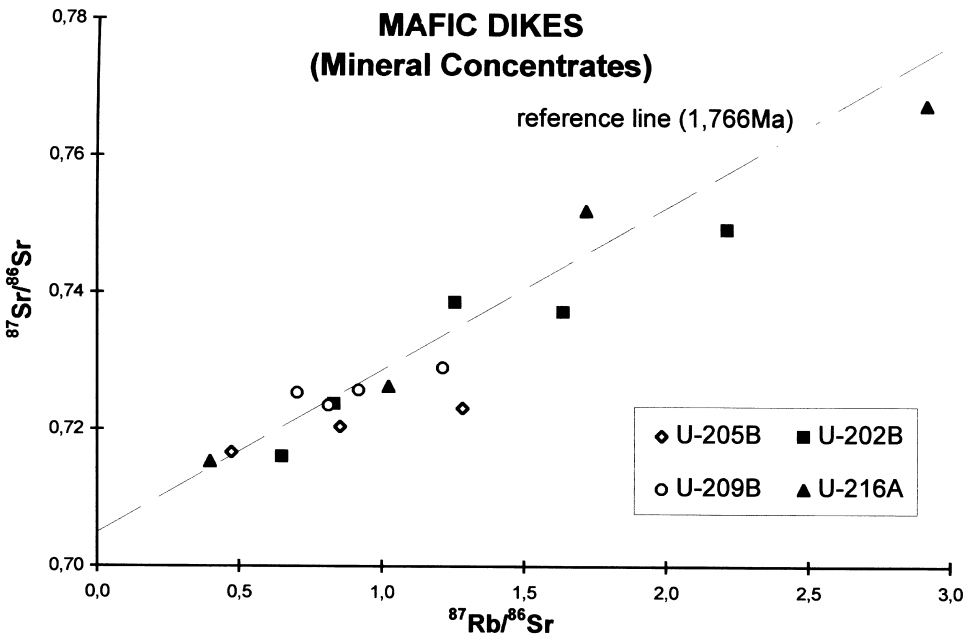

Fig. 11. Rb–Sr diagram data distribution for mineral concentrates analyzed (mafic dikes U-205B, U-202B, U-209B, U-216A) compared to the whole rock reference line of Fig. 9. See text for details.

(see Fig. 5). The anomalous slope of the line, controlled by the data plot of the HM fraction, suggests that this particular system probably has a higher Sr_0 than the other ones. A regression line was tentatively calculated for the F, M3 fractions and whole rock, yielding 1841 ± 138 Ma, $Sr_0 = 0.7038 \pm 0.0013$ and MSWD = 0.32 (Fig. 13). Although this age is compatible with the Rb–Sr

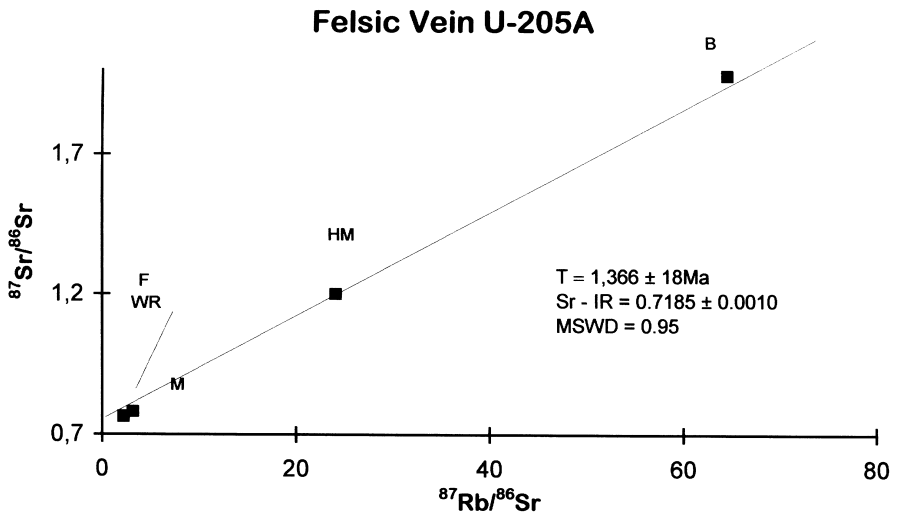

Fig. 12. Five-point isochron for felsic vein U-205A. B, Biotite; WR, whole rock; M, mafic, magnetic concentrate (>0.5 A); HM, hand magnet; F, felsic, less magnetic (<0.5 A) concentrate.

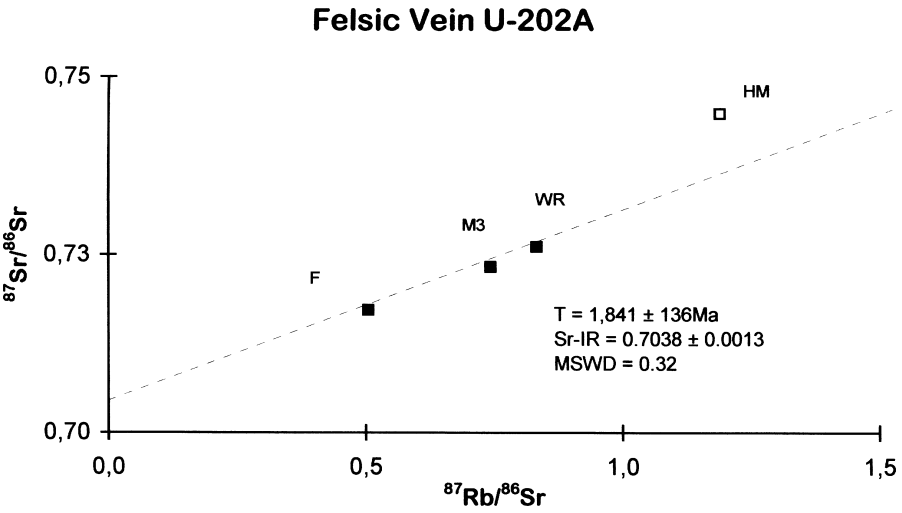

Fig. 13. Three-point isochron for felsic vein U-202A, excluding the HM fraction (□) from the age calculation. Selected samples: WR, M3 (>1.0 A) and F (<1.0 A) less magnetic Frantz concentrate. See text for explanation.

age of the UDS (Fig. 9), additional analyses are needed to better constrain the emplacement age of this felsic vein.

6. Tectonic implications

Geochronologic studies carried out on mafic dikes and felsic veins have refined the UDS emplacement age. Table 12 summarizes the significant isotopic data presently available for the dike swarm. The ^{40}Ar–^{39}Ar plateau ages on a micropegmatitic facies within the U-202 dike (high TiO_2 tholeiitic andesite) are 1727 ± 10 Ma (hornblende) and 1725 ± 10 Ma (biotite), the oldest of which provides the best estimate of the age of intrusion. The low TiO_2 group of dikes (andesitic basalts) were emplaced slightly earlier, associated with the

Table 12
Main geochronologic inferences from UDS samples (see text for details)

Rock	Age (Ma)	Type	Interpretation
Mafic dike (U-202)[a]	1727±10 (H) and 1725±10 (B)	Plateau ages[b]	Emplacement age
Mafic dikes	1766±124 (WR)	Best fit line[c] (15 dikes)	Emplacement age
Felsic vein (U-205)	1713±10 (M) and 1700±10 (B)	Plateau ages[b]	Emplacement age
Felsic vein (U-205A)	1366±18 (MSWD=0.95)	Mineral isochron[c]	Secondary thermal overprint
Felsic vein (U-203)	1169±13 (B) (low temperature discordance)	Isochron[a]	Secondary thermal overprint?
U-202	421±14 (B) (low temperature discordance)	Isochron[a]	Episodic outgassing or alteration

Observations: H, hornblende; B, Biotite; WR, whole rock.
[a]Low TiO_2 dike.
[b]^{40}Ar–^{39}Ar method.
[c]Rb–Sr method.

same regional crustal stress conditioning intrusion of the tholeiitic andesites. The felsic veins, intrusive into the UDS, are approximately contemporaneous with the youngest tholeiitic andesites, as indicated by ^{40}Ar–^{39}Ar plateau ages of 1713±10 Ma (muscovite) and 1710±10 Ma (biotite) on sample U-205A.

The UDS was intruded into a cold, Paleoproterozoic crust, in accordance with the K–Ar and ^{40}Ar–^{39}Ar radiometric pattern (2150–1817 Ma) shown by RLPC gneisses and granitoids. The integrated geochronologic and tectonic evidence point to an ensialic origin for the UDS (Bossi et al., 1993), herein interpreted as associated with a major aborted rift system within the newly formed Paleoproterozoic continental foreland. This tectonic setting, initiated soon after the Transamazonian orogeny, controlled the early formation of the rapakivi plutons between 1780 and 1750 Ma (Illescas, Minas de Corrales) followed by intrusion of the UDS (minimum age of 1727±10 Ma; see above). Evidence suggests that this rift system only reached the initial stages during which a fault-controlled basin was formed (Basal Group) mainly filled with epicratonic sediments and shallow-marine carbonates (Campal et al., 1995; Gaucher et al., 1996). A similar tectonic setting is postulated for the Tijucas basin located in the Nico Perez prolongation within southern Brazil.

Discordant post-emplacement Rb–Sr and ^{40}Ar–^{39}Ar ages of the UDS revealed that the isotopic systems have been variably disturbed (see Table 12). In particular, the felsic vein U-205A records a 1370 Ma secondary event that probably reached temperatures below 300°C. This idea is supported by the ^{40}Ar–^{39}Ar evidence available for this vein: the muscovite yields a flat plateau spectrum whilst the biotite that has lowest Ar closure temperature shows characteristically low temperature discordance. Additional evidence for secondary events is given by ^{40}Ar–^{39}Ar isochrons on felsic vein U-203 and mafic dike U-202 that yield ages of 1170 Ma and 420 Ma, respectively.

Nevertheless, because of the contrasting ages of rocks close to one another it was not possible to determine whether one or more events overprinted the western Uruguayan shield. In any case the isotopic disturbances could have overprinted extensive parts of the swarm, as suggested by the different geographic distribution of the samples. We speculate that reactivation of the fault systems which controlled the emplacement of the UDS could have been the probable mechanism through which low temperature hydrothermal fluids could promote disturbance of the isotopic systems. This interpretation is also consistent with the presence of some secondary mineralogy in the mafic dikes.

6.1. Chronology and correlations

Table 13 and Fig. 14 show selected geologic units (e.g. anorogenic plutonic and volcanic rocks, rift-related basins) located in the Brazilian Precambrian shield, that have radiometric ages between 1750 and 1680 Ma. These units are related

Table 13
Salient intraplate geologic features associated with the breakup of the Brazilian shield post-dating the Transamazonian orogeny

Geologic units	Ages (Ma)
Espinhaço rift (São Francisco Craton)	
A submeridional zone of extensional grabens and intracratonic basins, with subordinate felsic volcanism[a]	1752–1748 (± 4)[a]; 1711–1719 (± 2) [*a*]
Alkaline to subalkaline granitic suites[a] comparable with A-type magmatism of intraplate anorogenic environment (e.g. Borrachudos. São Timóteo)	1744 ± 2[a];
Contemporary felsic volcanism (Rio dos Remédios Group). Derivation from crustal sources: $\epsilon_{Nd} = -6$ and -10; $\mu_1 = 8.38$ and $^{87}Sr/^{86}Sr$ initial ratios >0.710	1729 ± 14 [*c*] 1730–1700 [*a*; *d*][a]
Amazonian Craton	
Basic sills, dikes and irregular masses of the Avanavero tholeiitic suite[a]. Intrusive relations with the Roraima cover	1670 ± 28 [*d*][a]
Undeformed felsic volcanism[a] of the Iriri Formation; association with subvolcanic plutons (including rapakivi rocks)[a]. Development of the Rio Negro–Juruena magmatic arc (1800–1550 Ma)	1790–1780 [*a*; *c*][a]
Rift-basins within Neoproterozoic polyclyclic domains	
Oros belt: shoshonitic basalts[a], subalkaline rhyolites[a] and gneisses[a]	1780–1700 [*a*][a]
Bimodal volcanism[a] at the base of the São Roque metavolcano-sediments	1790 [*a*][a]
Formation of the Araí–Natividade volcano[a]–sedimentary sequence; emplacement of granitoids[a] and mafic–ultramafic complexes[a]	~ 1770[a]–1720[a] [*a*; *c*]
Intrusion of rapakivi granites[a] and anorthosites (?) in the Nico Perez domain–Tijucas belt	1751–1760[a]

Geologic information and geochronologic data compiled from Hebeda et al. (1973); Basei (1978); Van Schmus et al. (1986); Macedo et al. (1988); Teixeira et al. (1989); Machado et al. (1989); Pimentel et al. (1991, 1994); Cordani et al. (1992); Babinski et al. (1994, 1996); Suita et al. (1994); Schobbenhaus et al. (1994); Dussin and Dussin (1995); Tassinari et al. (1996). See text for explanation.
[a]Selected rock units dated by: U–Pb on zircon [*a*]; Pb–Pb zircon evaporation [*b*]; Rb–Sr and Pb–Pb whole rock isochron [*c*]; K–Ar isochron [*d*].

to intraplate tectonics except for the Rio Negro–Juruena belt, a Paleo- to Mesoproterozoic magmatic arc in the Amazonian Craton, composed mainly of orthogneisses, migmatites and granitoid rocks (Tassinari et al., 1996).

The thick sedimentary sequences, acid to intermediate volcanism and subvolcanic plutons are associated either with incipient branching systems of rifts within the Paleoproterozoic landmasses (e.g. Amazonian Craton), or may evolve to large cratogenic basins filled with epicontinental to continental quartzite–pelite–carbonate assemblages (e.g. São Francisco Craton). Some of these basins were further involved in the fission of Rodinia supercontinent, during the initial steps of the Brazilian/Pan-African collages (ca 1 Ga ago) that finally led to the West Gondwana assembly.

The magnitude of the Late Paleoproterozoic igneous activity is exemplified within the Amazonian Craton by the Iriri volcanism that covers an area $>350\,000$ km^2 and the Avanavero tholeiitic suite (thick sills and sheeted dikes with total volumes of $30\,000$ km^3) intrusive into the Roraima Group (exposed area $>2\,500\,000$ km^2). This platform cover comprises thick sediments overlaying Transamazonian unmetamorphosed volcanic rocks located within the northern part of the craton (e.g. Hebeda et al., 1973; Basei, 1978; Teixeira et al., 1989; Brito Neves et al., 1995a).

The Late Paleoproterozoic metavolcano-sedimentary sequences related with rift-basins occur in the São Francisco Craton (Espinhaço Supergroup) and within the Neoproterozoic polycyclic domains where they crop out as relict basins (e.g. Orós, Araí-Natividade and São Roque rock associations) partly involved in the Brazilian orogenic framework. All these rock assemblages together with distinctive, contemporary plutonism

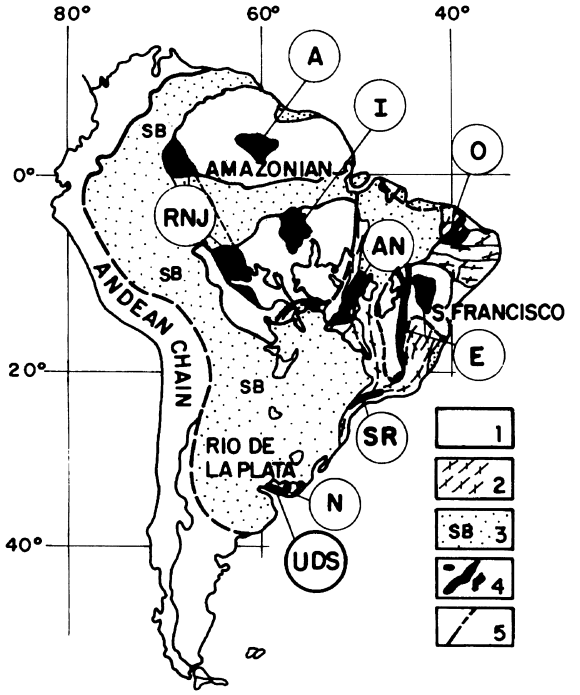

Fig. 14. Simplified geotectonic map of South America [adapted from Brito Neves et al. (1995a)] with the geographic location of the UDS and time-equivalent geologic units in Brazilian Precambrian shield. 1, Archean and Paleoproterozoic crust (including the Amazonian, São Francisco and Rio de la Plata cratons); 2, Neoproterozoic mobile belts; 3, Sub-Andean (SB) and Phanerozoic intracratonic basins. 4, Late Paleoproterozoic geologic features: UDS, Uruguayan dike swarm; N, Nico Perez domain (including Basal Group and Tijucas metasedimentary belt); E, Espinhaço system (Espinhaço Supergroup, Chapada Diamantina Group and chronocorrelative units); O, Orós belt; A, Avanavero suite; I, Iriri volcanism; RNJ, Rio Negro–Juruena belt. AN, Araí-Natividade volcano-sedimentary sequence; SR, São Roque belt; 5, major fault and lineaments. Dashed lines are boundaries between tectonic units.

(mafic–ultramafic suites; alkaline rocks, rapakivi granites, anorthosites) appear to be related with lithosphere thinness (cf Sengör, 1990) and point to a tendency to dispersion of continental fragments following their aggregation during the Transamazonian orogeny in South America.

The ~1.75 Ga Espinhaço Supergroup (Fig. 14), in particular, is a key-unit in understanding the geodynamic process at the end of the Paleoproterozoic, because the well-documented geologic record and the U–Pb geochronology available for the basal volcanic rocks. This aborted rift comprises a major continental to shallow marine, sedimentary sequence in greenschist metamorphic grade, with acid volcanism and granitic suites (~1.75–1.71 Ga; see Table 13) of metaluminous to sub-alkalic affinities emplaced within the rift's edge (e.g. Machado et al., 1989; Cordani et al., 1992; Pimentel et al., 1994; Babinski et al., 1994; Schobbenhaus et al., 1994; Dussin and Dussin, 1995).

The sedimentary characteristics of the Espinhaço Supergroup and Chapada Diamantina Group — a moderately folded cover — reveal a continuous memory of extensional, compressional, inversion and eustatic phases (Dominguez, 1993; Abreu, 1995). This complexity is also mirrored by isotopic disturbance of the Rb–Sr systematic (ca 1500–1280 Ma) on the granites, volcanics and basement rocks (e.g. Cordani et al., 1992). In a similar matter the Caboclo Formation (weakly deformed, recrystallized stromatolitic limestones), one of the Chapada Diamantina sequences, shows a Pb–Pb age of ca 1140 Ma (Babinski et al., 1993). This isotopic evidence is compatible with the occurrence of a superposed thermal event succeeding the basin formation (Cordani et al., 1992; Brito Neves et al., 1995a; Abreu, 1995). However, the presence of Late Mesoproterozoic overprints in the Espinhaço rift evolution is still open to controversy (e.g. Uhlein et al., 1995), since the radiometric ages may be a result of the isotopic systems which were partially opened during the Brazilian orogeny (750–500 Ma) when the rift structures were reactivated and strongly deformed.

Recent models for the Espinhaço rift have considered either the presence of an asthenospheric plume upwelling below the continental crust which allowed volcanism and vertical block movements (Abreu, 1995), or lithospheric thinning during the extensional phase (Dussin and Dussin, 1995). The latter extensional regime could cause upwelling of isotherms in the asthenosphere that finally led to decompression melting of the mantle sources and formation of the alkaline magmas.

The tectonic picture summarized above approximates that envisaged for the Late Paleoproterozoic evolution of the Uruguayan shield (and southernmost part of Brazil) because mafic and felsic

anorogenic magmatism (UDS, Illescas, Minas de Corrales), as well as fault-controlled basins (the Basal Group in the Nico Perez domain and Porongos Group in the Tijucas belt — see Section 2) occur in the area. The emplacement of the UDS can be therefore similarly related with the widespread extensional regime, represented by intraplate activity and basin sedimentation in South America, as already seen (Table 13). This leads to the conclusion that an extensional tectonic setting of transcontinental scale was predominant at the end of the Paleoproterozoic in South America. Our model also implies that distinctive magmatic rocks having a genetic relationship with the rapakivi suite (e.g. anorthosites, mangerites, charnockites, acid volcanics) can be expected within the Uruguayan shield. In this regard, it is noteworthy that the Capivarita meta-anorthosite, a 170 km^2 massive body cropping out in the Tijucas belt (not shown), yields a T_{DM} model age of 2.0 Ga and a calculated ϵ_{Nd} value of -0.5 for $T=1.7$ Ga [data in Babinski et al. (1997)].

On the other hand, the recognition of Late Mesoproterozoic orogenies (1300–1000 Ma) in South America is still dependent on detailed geologic mapping supported by U–Pb and Sm–Nd geochronology, except for recent work in the southwestern part of the Amazonian Craton (Sadowski and Bettencourt, 1996) and Northeast Brazil (Brito Neves et al., 1995b). Nevertheless, geologic correlation between southern South America and southern Africa, taking into account the Brazilian/Pan-African orogenies (e.g. Brito Neves and Cordani, 1991), allows a tectonic link for the Late Mesoproterozoic period with implications in the evolution of the RLPC.

In southern Africa Late Mesoproterozoic crustal evolution is well known, exemplified by the Namaqua orogeny (1300–1000 Ma), a 200–500 km wide plutonic and high–grade metamorphic belt extending for 2000 km across the southern flank of the Kaapvaal Craton, from the western Atlantic to the eastern Indian coast (Hartnady et al., 1985). In addition, as in the Uruguayan shield, the Paleoproterozoic (Transamazonian) crystalline basement played a critical role in controlling Namaqua evolution, represented by reflex intraplate activity (e.g., mafic dikes, granite suites, alkaline rocks, basin formation) and metamorphic episodes overprinted in the older terrains. In a Gondwana reconstruction, the Uruguayan shield lies within or close to the Namaqua belt and thus suggests that its evolution could have induced the post-emplacement ages that were obtained in some UDS rocks. Also we speculate that the ~1250 Ma crustal shortening recognized within the Nico Perez domain (e.g. Gaucher et al., 1996) could be a result of the Namaqua orogeny.

Finally, the above inferences provide new insights not only into the polycyclical orogenic history of the Uruguayan shield but also contributes to the paleotectonic reconstruction, preceding the Neoproterozoic rifting that evolved into the Gondwana–Laurentia breakup (e.g. Dalla Salda et al., 1992; Gaucher et al., 1996). Ongoing paleomagnetic studies on the UDS will help to test existing models on the assembly of Rodinia (Hoffman, 1991; Sadowski and Bettencourt, 1996), addressing a potential connection between the paleocontinent Plata and the southwestern part of the Amazonian Craton (Rondonia/Sunsás province) at the time of the Grenville orogeny.

Acknowledgment

The authors thank the CPGeo, São Paulo (Brazil) and Berkeley Geochronology Center (USA) for funding this project. They also acknowledge the logistic support given by the Instituto Astronômico e Geofísico of the University of São Paulo (Brazil) and the Faculdad de Agronomia (Uruguay). FAPESP (Brazilian Research Council Foundation) Grant Nos 91/1797-9, 92/3467-9 and 95/4652-2 supported field work and the analyses performed. They thank Nuno Machado, Richard Ernst, Thomas R. Fairchild and Marly Babinski for their reviews and suggestions in the manuscript and improvements in the language.

References

Abreu, P.A.A., 1995. O Supergrupo Espinhaço da Serra do Espinhaço Meridional (Minas Gerais): o rifte, a bacia e o orógeno. Geonomus 3 (1), 1–18.

Babinski, M., Van Scmus, R.W., Chemale Jr, F., Brito Neves, B.B., Rocha, A.J.D., 1993. Idade isocrônica Pb–Pb em rochas carbonáticas da formação Caboclo, em Morro do Chapéu. In: 2nd Symposium São Francisco Craton, extended abstract. SBG/SGM, Salvador, Brazil, pp. 160–163.

Babinski, M., Brito Neves, B.B., Machado, N., Noce, C.M., Uhlein, A., Van Schmus, R.W., 1994. Problemas da metodologia U/Pb em zircões de vulcânicas continentais: caso do grupo Rio dos Remédios, Supergrupo Espinhaço, no Estado da Bahia. In: Brazilian Geol Congr, extended abstract vol. 2. Camboriú, Brazil, pp. 409–410.

Babinski, M., Chemale , Jr, F., Hartmann, L.A., Van Schmus, W.R., Silva, L.C., 1996. Juvenile accretion at 750–700 Ma in Southern Brazil. Geology 24, 422–439.

Babinski, M., Chemale, Jr, F., Van Schmus, W.R., Hartmann, L.A., Silva, L.C., 1997. U–Pb and Sm–Nd geochronology of the Neoproterozoic granitic–gneissic Dom Feliciano Belt, Southern Brazil. J. S. Am. Earth Sci. 10 (3), (4), 263–274.

Baldwin, S.L., Harrison, T.M., Fitz Gerald, J.D., 1990. Diffusion of ^{40}Ar in metamorphic hornblende. Contrib. Mineral. Petrol. 105, 691–703.

Basei, M.A.S., 1978. O vulcanismo ácido-intermediário na região Amazônica. In: Brazilian Geol. Congr., An., vol. 30, No. 6. Recife, Brazil, pp. 2408–2422.

Bellieni, G., Petrini, R., Piccirillo, E.M., Cavazzini, G., Civetta, L., Comin-Chiaramonti, P., Melfi, A.J., Bertolo, S., De Min, A., 1991. Proterozoic mafic dike swarm of the São Francisco Craton (SE-Bahia, Brazil): petrology and Sr–Nd isotopes. Eur. J. Mineral. 3, 429–449.

Bellieni, G., Petrini, R., Girardi, V.A.V., Menezes Leal, A.B., Teixeira, W., Bastos Leal, L.R., De Min, A., Piccirillo, E.M., 1995. Petrological and Sr–Nd evidence bearing on Early Proterozoic magmatic events of the subcontinental mantle: São Francisco Craton (Uauá, NE-Brazil). Contrib. Mineral. Petrol. 122, 252–261.

Bossi, J., 1983. Breve reseña sobre el conocimiento geológico del Escudo Predevoniano en Uruguay (Sud América). Zentralbatte Sur. Geol. Palaont. I (3), (4), 417–429.

Bossi, J., Campal, N., 1991. Granitos negros filonianos del Uruguay: resultados de las investigaciones. Agreement Canadá–Universidade de la República–Faculdad de Agronomia (Uruguay). Centro Internacional de Investigacion para el desarrollo. Montevideo, Uruguay.

Bossi, J., Campal, N., 1992. Magmatismo y tectonica transcurrente durante el Paleozoico Inferior en Uruguay. In: Gutiérrez Marco, J.G., Saavedra, J., Rábano, I. (Eds.), Paleozoico inferior de Ibero-America. IUGS/UNESCO, pp. 343–356.

Bossi, J., Navarro, R., 1988. Geologia del Uruguay. Universidad de La Republica. vol. 1. Montevideo, Uruguay.

Bossi, J., Campal, N., Civetta, L., Demarchi, G., Girardi, V.A.V., Mazzucchelli, M., Negrini, L., Rivalenti, G., Fragoso Cesar, A.R.S., Sinigoi, S., Teixeira, W., Piccirillo, E.M., Molesini, M., 1993. Early Proterozoic dike swarms from western Uruguay: geochemistry, Sr–Nd isotopes and petrogenesis. Chem. Geol. 106 (3), (4), 263–277.

Bossi, J., Mutti, D., Piñeyro, D., Di Marco, A., 1996. El Cinturon Arqueano Uruguayo de San Jose: caracterizacion litogeoquimica de su area tipo. In: XIII Congresso Geologico Argentino, vol. III. San Juan, Argentina, pp. 567–579.

Brito Neves, B.B., Cordani, U.G., 1991. Tectonic evolution of South America during the Late Proterozoic. Precambrian Res. 53 (1/2), 23–40.

Brito Neves, B.B., Sá, J.M., Nilson, A.A., Botelho, N.F., 1995a. A trafogênese estateriana nos blocos paleoproterozóicos da América do Sul e processos subsequentes. Geonomus, Rev. Geoc. 3 (2), 1–21.

Brito Neves, B.B., Van Schmus, W.R., Santos, E.J., Campos Neto, M.C., Kozuch, M., 1995b. O evento Cariris Velhos na província Borborema: integração de dados, implicações e perspectivas. Rev. Bras. Geoc. 25 (4), 279–296.

Campal, J., 1990. Aportes al conocimiento de la estratigrafia durante el precambrico medio del Uruguay. In: Congresso Uruguayo de Geologia, vol. I. Montevideo, Uruguay, pp. 65–70.

Campal, N., Garat, I., 1990. Consecuencias petrológicas de las variaciones composicionales dentro del Haz de filones máficos precambrianos del centro-sur del Uruguay. In: Workshop 'Diques máficos do Brasil', vol. II. IGCP-257/IGc-USP. São Paulo, Brazil, pp. 99–109.

Campal, N., Schipilov, A., 1995. The Illescas Bluish Quartz Rapakivi granite (Uruguay–South America): some geological features. In: Symp. Rapakivi Granites and Related Rocks. IGCP project 315. Abstract vol. 18. Belém, Brazil.

Campal, N., Gaucher, C., Schipilov, A., Bossi, J., 1995. El Uruaçuano en el Uruguay: evidencias geologicas, paleontologicas y radimetricas. In: 6 Simp. Sul-Brasileiro de Geologia. Bol. res. expandidos. Porto Alegre, Brazil, pp. 97–99.

Cingolani, C.A., Bossi, J., Varela, R., Navarro, R., 1990. Nuevos datos geológicos y geocronológicos del macizo granítico de Cerro Colorado, Florida, Uruguay. In: Uruguayan Geol. Congr., vol. I. Montevideo, Uruguay, pp. 101–106.

Cingolani, C.A., Varela, R., Dalla Salda, L., Bossi, J., Campal, N., Ferrando, L., Piñeyro, D., Schipilov, A., 1997. Rb–Sr geochronology from the Rio de La Plata craton of Uruguay. In: South American Symposium on Isotope Geology. Extended Abstract. Campos do Jordão, Brazil, pp. 73–75.

Cordani, U.G., Soliani, E., , Jr1990. Idades K–Ar e Rb–Sr das 'Ilhas Cristalinas' de Rivera e Aceguá (Uruguai e Rio Grande do sul, Brasil) e seu enquadramento no contexto geotectônico regional. An. Acad. bras. Ci. 62 (2), 145–156.

Cordani, U.G., Halpern, M., Berenholc, M., 1974. Comentários sobre as determinações geocronológicas da Folha Porto Alegre. In: Carta Geológica do Brasil ao Milionésimo. Folha Porto Alegre-SH.22 e Folha Lagoa Mirim-SI.22. DNPM/MME. Brasília, pp. 70–88.

Cordani, U.G., Teixeira, W., Tassinari, C.C.G., Kawashita, K., Sato, K., 1988. The growth of the Brazilian Shield. Episodes 11 (3), 163–167.

Cordani, U.G., Kawashita, K., Sato, K., Iyer, S.S., Taylor, P.N., 1992. Pb–Pb, Rb–Sr and K–Ar systematics of the Lagoa Real Uranium Province (South Central Bahia, Brazil)

and the Espinhaço orogeny (ca. 1.5–1.0 Ga). J. S. Am. Earth Sci. 5 (1), 33–36.

D'Agrella Filho, M.S., Pacca, I.I.G., Renne, P.R., Onstott, T.C., Teixeira, W., 1990. Paleomagnetism of Middle Proterozoic (1.01 to 1.08 Ga.) mafic dykes in Southeastern Bahia State–São Francisco Craton, Brazil. Earth Planet. Sci. Lett. 101, 332–348.

D'Agrella Filho, M.S., Pacca, I.I.G., Teixeira, W., Renne, P.R., 1997. Magnetic characterization of the 1.73 Ga mafic dikes form the Rio de la Plata Craton, Uruguay. Int. Geology Rev. submitted.

Dalla Salda, L.H., Bossi, J., Cingolani, C.A., 1988. The Rio de la Plata Cratonic Region of Southwestern Gondwanaland. Episodes 11 (4), 263–269.

Dalla Salda, L., Cingolani, C., Varela, R., 1992. Early Paleozoic orogenic belt of the Andes in southwestern South America: result of Laurentia–Gondwana collision? Geology 20, 617–620.

Deino, A., Potts, A., 1990. Single-crystal $^{40}Ar/^{39}Ar$ dating of the Olorgesailie Formation, Southern Kenya Rift. J. Geophys. Res. 95 (B6), 8453–8470.

Dominguez, J.M.L., 1993. As coberturas do Cráton do São Francisco: uma abordagem do ponto de vista de análise de bacias. In: Dominguez, J.M.L., Misi, A. (Eds.), O Cráton do São Francisco. Salvador, Brazil. SBG/SGM/CNPq, pp. 137–160.

Dussin, I.A., Dussin, T.M., 1995. Supergrupo Espinhaço: modelo de evolução geodinâmica. Geonomus, Rev. Geoc. III (1), 19–26.

Fernandez, A., Preciozzi, E., 1974. La Formacion Arroyo Grande y los granitoides asociados. In: Brazilian Geol. Congr., An., vol. 28. Porto Alegre, Brazil, pp. 213–226.

Ferrando, L.A., Fernandez, R.N., 1971. Esquema tectônico cronoestratigráfico del Predevoniano en Uruguay. In: Brazilian Geol. Congr., vol. 25, No. 1. São Paulo, Brazil, pp. 199–210.

Fleck, R.J., Sutter, J.F., Elliot, D.H., 1977. Interpretation of discordant $^{40}Ar/^{39}Ar$ age-spectra of Mesozoic tholeiites from Antarctica. Geochim. Cosmochim. Acta 41, 15–32.

Fragoso Cesar, A.R.S., 1991. Tectônica de placas no ciclo Brasiliano: As orogenias dos cinturões Dom Feliciano e Ribeira no Rio Grande do Sul. Doctoral thesis, Institute of Geosciences, USP, São Paulo.

Gaucher, C., Sprechmann, P., 1995. Paleontologia, sedimentologia y paleogeografia del Proterozoico medio y superior del terreno Nico Perez, Uruguay. In: 6 Simp. Sul-Brasileiro Geol., Bol. res. expandidos. Porto Alegre, Brazil, pp. 101–104.

Gaucher, C., Sprechmann, P., Schipilov, A., 1996. Upper and Middle Proterozoic fossiliferous sedimentary sequences of the Nico Pérez Terrane of Uruguay: lithostratigraphic units, paleontology, depositional environments and correlations. Neues Jahrbuch für Geologie und Paleontologie, Abhandlung 199 (3), 339–367.

Gomez Rifas, C., 1988. La edad de los microgabbros negros del Proterozoico medio del Uruguay. In: Reunion Geol. Uruguay. Acta I, Salto, Uruguay, pp. 106–107.

Gurnis, M., 1988. Large-scale mantle convection and the aggregation and dispersal of supercontinents. Nature 332, 695–699.

Hallinan, S.E., Shukowsky, W., Mantovani, M.S.M., 1993. Estruturação do embasamento pré-cambriano na região sul do Brasil e Uruguay. Novos modelos resultantes de classificação gravimétrica. In: Primer Simposio Internacional del NeoProterozoico-Cambriano de La Cuenca del plata. Res. Extensos, Tomo II. Montevideo, Uruguay.

Harrison, T.M., Duncan, I., McDougall, I., 1985. Diffusion of ^{40}Ar in biotite: temperature, pressure and composition effects. Geochim. Cosmochim. Acta 49, 2461–2468.

Hart, S., 1966. Radiometric ages in Uruguay and Argentina and their implications concerning Continental Drift. Geol. Soc. America Special Paper, Bull. 101, 86

Hartnady, C., Joubert, P., Stowe, C., 1985. Proterozoic crustal evolution in southwestern Africa. Episodes 8 (2), 236–244.

Hebeda, E.H., Boelrijk, N.A.I.M., Priem, H.N.A., Verdumen, E.A.Th., Verschure, R.H., 1973. Excess radiogenic argon in the Precambrian Avanavero Dolerite in Western Suriname (South America). Earth Planet. Sci. Lett. 20, 189–200.

Hoffman, P.F., 1991. Did the breakout of laurentia turn Gondwanaland inside-out? Science 252, 1409–1412.

Logan, B.W., Rezak, R., Tappan, H., 1964. Classification and environmental significance of algal stromatolites. J. Geol. 72, 62–83.

Macedo, M.H.F., Sá, J.M., Kawashita, K., 1988. A idade da faixa Orós: dados preliminares. Rev. Bras. Geoc. 18 (3), 1–24.

Machado, N., Schrank, A., Abreu, F.R., Knauer, L.G., Almeida Abreu, P.A., 1989. Resultados preliminares da geocronologia U/Pb na Serra do Espinhaço Meridional. In: Anais, V Simp. Geol. Núcleo M.G. and I Simp. Geol. Núcleo Brasília, SBG, Belo Horizonte, Bol. 10, pp. 171–174.

Mazzucchelli, M., Rivalenti, G., Piccirillo, E.M., Girardi, V.A.V., Civetta, L., Petrini, R., 1995. Petrology of the Proterozoic mafic dyke swarms of Uruguay and constrains on their mantle source composition. Precambrian Res. 74, 177–194.

Onstott, T.C., Hall, C.M., York, D., 1989. $^{40}Ar/^{39}Ar$ thermochronology of the Imataca Complex, Venezuela. Precambrian Res. 42, 255–291.

Pimentel, M.M., Heaman, I., Fuck, R.A., Marini, O., 1991. U–Pb zircon geochronology of Precambrian tin-bearing continental-type acid magmatism in central Brazil. Precambrian Res. 52, 321–335.

Pimentel, M.N., Machado, N., Lobato, L.M., 1994. Geocronologia U–Pb de rochas graníticas da região de Lagoa Real, Bahia. In: Brazilian Geol. Congr., vol. 38. Extended abstract, vol. 2. Camboriú, Brazil, pp. 389–390.

Precciozi, F., Bourne, J.H., 1992. Petrography and geochemistry of the Arroyo de la Virgen and Isla Mala plutons, southern Uruguay: Early Proterozoic tectonic implications. J. S. Am. Earth Sci. 6 (3), 169–181.

Renne, P.R., Onstott, T.C., D'Agrella-Filho, M.S., Pacca, I.G., Teixeira, W., $^{40}Ar/^{39}Ar$ dating of 1.0–1.1 Ga magnetizations from the São Francisco and Kaapvaal Cratons: tectonic

implications for Pan-African and Brasilian Mobile belts. 1990. Earth Planet. Sci. Lett. 101, 349–366.

Renne, P.R., Deino, A.L., Walter, R.C., Turrin, B.D., Swisher, C.C., Becker, T.A., Curtis, G.H., Sharp, W.D., Jaouni, A.-R., 1994. Intercalibration of astronomical and radioisotopic time. Geology 22, 783–786.

Renne, P.R., Deckart, K., Ernesto, M., Féraud, G., Piccirillo, E.M., 1996. Age of the Ponta Grossa Dike Swarm (Brazil) and implications for the Paraná Flood Volcanic Province. Earth Planet. Sci. Lett. 144, 199–212.

Renne, P.R., Swisher, C.C., Deino, A.L., Owens, T., DePaolo, D.J., Karner, D.B., 1998. Intercalibration of standards, absolute ages and uncertainties in $^{40}Ar/^{39}Ar$ dating. Chem. Geol. (Isot. Geosci. Sect.) 154 (1), (2), 117–152.

Rivalenti, G., Girardi, V.A.V., Bossi, J., Campal, N., Civetta, L., Mazzuchelli, M., Molesini, M., Linari, S., Teixeira, W., 1991. Petrology and geochemistry of Precambrian dyke swarms of Uruguay. In: Int. Symp. on Mafic Dykes Extended Abstr. São Paulo, Brazil, pp. 41–46.

Sadowski, G.R., Bettencourt, J.S., 1996. Mesoproterozoic tectonic correlations between eastern Laurentia and the western border of Amazonian craton. Precambrian Res. 76, 213–227.

Schobbenhaus, C., Hoppe, A., Baumann, A., Lork, A., 1994. Idade U–Pb do vulcanismo Rio dos Remédios, Chapada Diamantina, Bahia. In: Brazilian Geol. Congr., 38. Extended Abstract, vol. 2. Camburiú, Brazil, pp. 397–399.

Sengör, A.M.C., 1990. Plate tectonics and orogenic research after 25 years: a Tethyan perspective. Earth Sci. Rev. 27, 1–201.

Soliani, E. Jr, 1986. Os dados geocronológicos do escudo Sul-Riograndense e suas implicações de ordem geotectônica. Doctoral thesis. Institute of Geosciences. University of São Paulo, São Paulo, Brazil.

Steiger, R.H., Jäger, E., 1977. Subcomission on geochronology: convention on the use of decay constants in geo- and cosmochronology. Earth Planet. Sci. Lett. 36, 359–362.

Suita, M.F.T., Kamo, S.L., Krogh, T.E., Fyfe, W.S., Hartmann, L.A., 1994. U–Pb ages from the high-grade Barro Alto mafic–ultramafic complex (Goiás, Central Brazil): Middle Proterozoic continental mafic magmatism and Upper Proterozoic continental collision. In: Int. Conf. on Geochronology, Cosmochronology and Isotope Geology. Abstract vol. 8. Berkeley, USA, p. 309.

Tassinari, C.C.G., Cordani, U.G., Nutman, A.P., Van Schmus, W.R., Bettencourt, J.S., Taylor, P.N., 1996. Geochronological systematics on basement rocks from the Rio Negro–Juruena province (Amazonian Craton) and tectonic implications. Int. Geol. Rev. 38, 161–175.

Teixeira, W., Tassinari, C.C.G., Cordani, U.G., Kawashita, K., 1989. A review of the geochronology of the Amazonian craton: teconic implications. Precambrian Res. 42, 213–227.

Uhlein, A., Trompette, R., Egydio-Silva, M., 1995. Rifteamentos superpostos e tectônica de inversão na borda sudeste do Cráton do São Francisco. Geonomos 3 (1), 99–107.

Umpierre, M., Halpern, M., 1971. Edades estroncio-rubidio en rocas cristalinas del sur de la Republica Oriental del Uruguay. Rev. Assoc. Geol. Argentina 26 (2), 133–155.

Van Schmus, W.R., Tassinari, C.C.G., Cordani, U.G., 1986. Estudo geocronológico da parte inferior do Grupo São Roque. In: Brazilian Geol. Congress 34, An., vol. 3, Goiânia, Brazil, pp. 1390–1405.

Williamson, J.H., 1968. Least-squares fitting of a straight line. Can. J. Phys. 46, 1845–1847.

Windley, B.F., 1984. The Evolving Continents, 2nd edn. Wiley, New York.

Zen, E., Hammarstrom, J.M., 1984. Magmatic epidote and its petrologic significance. Geology 12, 515–518.